https://doi.org/10.1093/plcell/koad210 THE PLANT CELL 2023: 35: 4020–4045

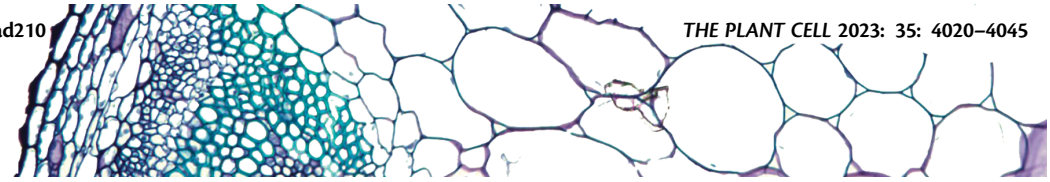

Research Article

Deciphering the regulatory network of the NAC transcription factor FvRIF, a key regulator of strawberry (*Fragaria vesca*) fruit ripening

Xiaojing Li [1,2,3] Carmen Martín-Pizarro [4] Leilei Zhou [1,2] Bingzhu Hou [1] Yuying Wang [1,2] Yuanyue Shen [5] Bingbing Li [6] David Posé [4,*] and Guozheng Qin [1,2,3,*,†]

1 Key Laboratory of Plant Resources, Institute of Botany, Chinese Academy of Sciences, Beijing 100093, China
2 China National Botanical Garden, Beijing 100093, China
3 University of Chinese Academy of Sciences, Beijing 100049, China
4 Instituto de Hortofruticultura Subtropical y Mediterránea (IHSM), Universidad de Málaga-Consejo Superior de Investigaciones Científicas, Departamento de Biología Molecular y Bioquímica, Facultad de Ciencias, UMA, Málaga 29071, Spain
5 College of Plant Science and Technology, Beijing University of Agriculture, Beijing 102206, China
6 College of Horticulture, China Agricultural University, Beijing 100193, China

*Author for correspondence: gzqin@ibcas.ac.cn (G.Q.), dpose@uma.es (D.P.)
†Senior author.
The author responsible for the distribution of materials integral to the findings presented in this article in accordance with the policy described in the Instructions for Authors (https://academic.oup.com/plcell) is: gzqin@ibcas.ac.cn.

Abstract

The NAC transcription factor ripening inducing factor (RIF) was previously reported to be necessary for the ripening of octoploid strawberry (*Fragaria* × *ananassa*) fruit, but the mechanistic basis of RIF-mediated transcriptional regulation and how RIF activity is modulated remains elusive. Here, we show that FvRIF in diploid strawberry, *Fragaria vesca*, is a key regulator in the control of fruit ripening and that knockout mutations of *FvRIF* result in a complete block of fruit ripening. DNA affinity purification sequencing coupled with transcriptome deep sequencing suggests that 2,080 genes are direct targets of FvRIF-mediated regulation, including those related to various aspects of fruit ripening. We provide evidence that FvRIF modulates anthocyanin biosynthesis and fruit softening by directly regulating the related core genes. Moreover, we demonstrate that FvRIF interacts with and serves as a substrate of MAP kinase 6 (FvMAPK6), which regulates the transcriptional activation function of FvRIF by phosphorylating FvRIF at Thr-310. Our findings uncover the FvRIF-mediated transcriptional regulatory network in controlling strawberry fruit ripening and highlight the physiological significance of phosphorylation modification on FvRIF activity in ripening.

Introduction

Strawberries (*Fragaria* spp.) are important fleshy fruits with high economic value worldwide due to their attractive appearance, delicious taste, and nutritional value (Basu et al. 2014; Giampieri et al. 2014). The nutritional composition of strawberry fruits includes micronutrients, such as vitamin C, minerals, and folates, and nonnutrient elements, such as phenolic compounds, which are beneficial for human health (Giampieri et al. 2014). The cultivated species is commonly the octoploid strawberry *Fragaria* × *ananassa*, in which gene function analysis is challenging due to its quite complicated genetic background (Edger et al. 2019). By contrast, the diploid woodland strawberry (*Fragaria vesca*), which possesses a much simpler genetic background, short life cycle, and mature transgenic systems, has emerged as a model system for studying fruit development and quality in nonclimacteric fruits.

Ripening is a complex process in the final phase of fruit development. The formation of fruit quality, including color,

Received May 22, 2023. Accepted July 02, 2023. Advance access publication July 28, 2023

IN A NUTSHELL

Background: Strawberry is an important horticultural crop with a high economic value worldwide. Various factors regulate the ripening of strawberry fruit, including the plant hormone abscisic acid (ABA), epigenetic modifications, and transcription factors. In a previous study, the transcription factor ripening inducing factor (RIF) was reported to be necessary for the ripening of strawberry fruit, but the regulatory network mediated by RIF remains unclear.

Question: What are the direct target genes of RIF in strawberry? How is the transcriptional activity of RIF modulated?

Findings: We found that RIF in diploid strawberry (*Fragaria vesca*, FvRIF) functions as a key regulator in controlling fruit ripening, and loss of function of FvRIF leads to a complete blockage of the ripening process. DNA affinity purification sequencing coupled with RNA sequencing identified 2,080 genes as potential direct targets of FvRIF, including genes involved in anthocyanin biosynthesis, cell-wall degradation, and sugar metabolism. We demonstrate that FvRIF regulates various aspects of fruit ripening by directly modulating core sets of genes involved in these processes. Furthermore, we show that FvRIF physically interacts with the kinase FvMAPK6, which phosphorylates and regulates FvRIF activity.

Next steps: We next wish to identify the transcription factors that directly bind to the promoter of *FvRIF* and regulate its expression. Moreover, our work suggests a number of transcription factors as the targets of FvRIF. It will be interesting to explore their function in the regulation of strawberry fruit ripening.

texture, flavor, and aroma, is determined by ripening (Fenn and Giovannoni 2021). A better understanding of the mechanistic basis underlying fruit ripening will not only facilitate genetic engineering for the control of ripening but will also promote the development of new strategies for the improvement of fruit quality or extension of fruit shelf life. The ripening of strawberry, a classical nonclimacteric fruit, is regulated by various factors, among which the plant hormone abscisic acid (ABA) acts as a critical regulator, manipulating the expression of genes that determine quality attributes. ABA affects multiple physiological responses throughout strawberry fruit ripening, and its concentration increases along with fruit ripening progression (Chai et al. 2011; Jia et al. 2011; Ji et al. 2012; Jia et al. 2013; Chai and Shen 2016). In addition to ABA, epigenetic modifications, including DNA 5-methylcytosine (5mC) methylation and mRNA N^6-methyladenosine (m^6A) methylation, also play an important role in the regulation of strawberry fruit ripening (Cheng et al. 2018). In recent years, a number of transcription factors (TFs) have been identified and functionally characterized as regulators of fruit ripening or quality formation in strawberry (Sanchez-Gomez et al. 2022). For example, FaMYB10 and FaMYB1, members of the R2R3-type MYB TF family, regulate the biosynthesis of phenylpropanoids, flavonoids, and anthocyanins in strawberry fruit (Aharoni et al. 2001; Lin-Wang et al. 2010; Medina-Puche et al. 2014). The MADS-box proteins FaMADS9 and FaSHP (SHATTERPROOF) are associated with strawberry development and ripening (Seymour et al. 2011; Daminato et al. 2013), while the MYB and DNA binding with One Finger (DOF)-like TFs FaEOBII (Emission of Benzenoid II) and FaDOF2 can promote the biosynthesis of eugenol, a volatile phenylpropanoid in ripe strawberry (Koeduka et al. 2006; Molina-Hidalgo et al. 2017). Despite the significance of TFs in the control of fruit ripening and acquisition of quality traits, high-throughput identification of TF binding sites has not been reported in strawberry, probably due to the technical challenges caused by the complex metabolite components present in strawberry. Thus, our understanding of the transcriptional regulatory networks regarding strawberry fruit ripening and how these TFs orchestrate ripening is still very limited.

NAC (NAM, ATAF, and CUC) TFs constitute a family of TFs specific to plants, with more than 100 members in *Arabidopsis* (*Arabidopsis thaliana*) (Riechmann et al. 2000). Most NAC proteins contain a conserved N-terminal DNA-binding domain (BD) and a variable C-terminal domain (Olsen et al. 2005). Recently, a NAC TF, FaRIF (ripening inducing factor), was reported as an essential positive regulator of fruit ripening in octoploid strawberry, as revealed by the numerous ripening-related responses that were altered after the repression of *FaRIF* expression by RNA interference (RNAi) (Martin-Pizarro et al. 2021). However, the direct targets modulated by FaRIF and the mechanisms underlying FaRIF-mediated transcriptional regulation are poorly understood. Moreover, how FaRIF activity is regulated has not been uncovered. Such information is critical to elucidate the regulatory cascade controlled by FaRIF and to understand the connections with other regulatory networks controlling strawberry fruit ripening.

Due to the critical role of TFs in controlling gene expression in diverse biological contexts, their activity needs to be tightly regulated. Posttranslational modifications, including phosphorylation, SUMOylation, ubiquitination, acetylation, glycosylation, and methylation, represent an important layer of regulation for TF activity (Filtz et al. 2014). Such modifications can rapidly and reversibly modulate virtually all aspects of TF activity, such as stability, subcellular localization, transcriptional activities, and interactions with cofactors. Among the extensively studied posttranslational modifications, phosphorylation appears to

be a ubiquitous mechanism that affects TF activity. Protein phosphorylation, which may occur at serine (S or Ser), threonine (T or Thr), or tyrosine (Y or Tyr) residues, is catalyzed by protein kinases including MAP kinases (MAPKs), receptor-like kinases, calcium-dependent protein kinases (CDPKs), and sucrose nonfermenting1–related protein kinases 2 (SnRK2s) (Komis et al. 2018; Yip Delormel and Boudsocq 2019; Soma et al. 2020). Although substantial advances have been achieved in understanding the regulatory effects of protein phosphorylation on the activity of TFs in model plants such as *Arabidopsis*, relatively little information is known in horticultural crops so far.

In the present study, we generated stable knockout mutants of *FvRIF*, the ortholog of *FaRIF* in diploid *F. vesca*, using a clustered regularly interspaced short palindromic repeat (CRISPR)/CRISPR-associated nuclease 9 (Cas9)-mediated gene editing, and showed that *FvRIF* functions as a master regulator in controlling strawberry fruit ripening. Compared to the *FaRIF*-RNAi lines (Martin-Pizarro et al. 2021), the mutants display a more severe ripening-inhibited phenotype whereby fruits never turn red, indicating that the flexible application of CRISPR/Cas9 gene-editing approach is an efficient strategy to explore gene function in strawberry. A DNA affinity purification sequencing (DAP-seq) approach coupled with transcriptome deep sequencing (RNA sequencing [RNA-seq]) analysis suggests that FvRIF directly regulates 2,080 genes involved in various aspects of fruit ripening, such as anthocyanin biosynthesis, cell-wall degradation, and sugar metabolism. Furthermore, we demonstrate that FvRIF physically interacts with the kinase FvMAPK6, which phosphorylates and regulates the transcriptional activity of FvRIF. Thus, our study contributes to the understanding of the transcriptional regulatory network mediated by FvRIF and uncovers links between protein translational modification and TF activity.

Results

FvRIF functions as a master regulator in the control of strawberry fruit ripening

We identified FvRIF (FvH4_3g20700), the ortholog of FaRIF from *F.* × *ananassa* (maker-Fvb3-4-augustus-gene-182.31), in the genome of the diploid strawberry, showing 100% protein sequence identity with FaRIF (Supplemental Fig. S1). A phylogenetic analysis showed that FvRIF is most closely related to CmNAC-NOR (nonripening) from melon (*Cucumis melo*) and CsNAC56 from sweet orange (*Citrus sinensis*), followed by SlNOR and SlNOR-like1 from tomato (*Solanum lycopersicum*) and NtNAC56-like in tobacco (*Nicotiana tabacum*) (Fig. 1A). We analyzed *RIF* expression in *F. vesca* and *F.* × *ananassa* by reverse transcription quantitative PCR (RT-qPCR), showing that *FvRIF* is highly expressed in fruits and increases during ripening in diploid strawberry (Fig. 1B), similar to *FaRIF* in octoploid strawberry (Fig. 1C). Notably, besides *FvRIF*, there are 11 additional homologous genes that share greater than 50% sequence similarity with *FaRIF* (Supplemental Fig. S2A). Expression analysis of these homologous genes in various tissues and ripening in *F. vesca* revealed that 5 of these genes are not detectably expressed, while the remaining 6 genes are expressed at differential levels (Supplemental Fig. S2B).

To fully investigate the function of *FvRIF* in strawberry, we generated stable *FvRIF* knockout mutants in diploid strawberry (*F. vesca* cv. Ruegen) using CRISPR/Cas9-mediated gene editing. We used 2 single guide RNA (sgRNA) expression cassettes containing different target sequences (T1 and T2) to specifically target the first exon of *FvRIF* (Fig. 1D). After transformation, we genotyped the positive seedlings obtained based on hygromycin resistance by PCR, followed by DNA sequencing. We identified 3 independent homozygous mutant lines (*Fvrif-1*, *Fvrif-6*, and *Fvrif-13*) in the second generation. Lines *Fvrif-1* and *Fvrif-6* harbored a 1- and 40-bp deletion, respectively, while line *Fvrif-13* carried 2 deletions of 1 and 25 bp (Fig. 1E). All mutants were predicted to produce nonfunctional truncated FvRIF proteins. We chose the mutant lines *Fvrif-6* and *Fvrif-13* with longer deletions for analysis. Immunoblot analysis using an affinity-purified specific anti-FvRIF polyclonal antibody generated in this study detected a band corresponding to the predicted size (~38 kD) of the full-length FvRIF only in the wild type, but not in the *Fvrif-6* or *Fvrif-13* mutant lines, indicating that *FvRIF* is successfully knocked out in these lines (Figs. 1F and S3). We predicted potential off-target sites in the strawberry genome by CRISPR-P (version 2.0, http://crispr.hzau.edu.cn/CRISPR2/). Of the 3 potential off-target sites identified, 2 are located in intergenic regions, and 1 is located in the coding region of FvH4_6g41601. We genotyped the sequences containing these potential off-target sites through direct sequencing of the PCR products from genomic DNA flanking the potential target sites. We detected no mutation in any of the 3 potential off-target sites (Supplemental Fig. S4), suggesting the specific mutation for *FvRIF*.

Fvrif-6 and *Fvrif-13* mutant lines displayed similar and clear inhibition of ripening phenotypes (Fig. 1G). The fruits in the mutants failed to fully ripen and remained white at the final ripe stage (Figs. 1G and S5, A to C), suggesting that FvRIF acts as a master regulator in controlling strawberry fruit ripening. Consistent with the color phenotype, the anthocyanin content decreased by >90% in fruits of the *Fvrif* lines at 28 d postanthesis (DPA) (Fig. 1H). By contrast, fruit softening was markedly inhibited in the *Fvrif* lines, which exhibited approximately 18-fold higher fruit firmness compared to the wild type (Fig. 1I). Moreover, levels of the major sugars were altered in fruits of the *Fvrif* lines, with significantly lower levels for sucrose, glucose, and fructose compared to the wild type (Fig. 1J). *Fvrif-1* only exhibited a slight delay in fruit ripening (Supplemental Fig. S6), probably due to its 1-bp deletion.

To confirm the positive role of FvRIF in the regulation of *F. vesca* fruit ripening, we also generated stable *FvRIF* overexpression lines (*FvRIF*-OE-L20 and *FvRIF*-OE-L21) in diploid strawberry: these overexpression lines displayed phenotypes opposite to those seen in the *Fvrif* lines (Fig. 1, G to J).

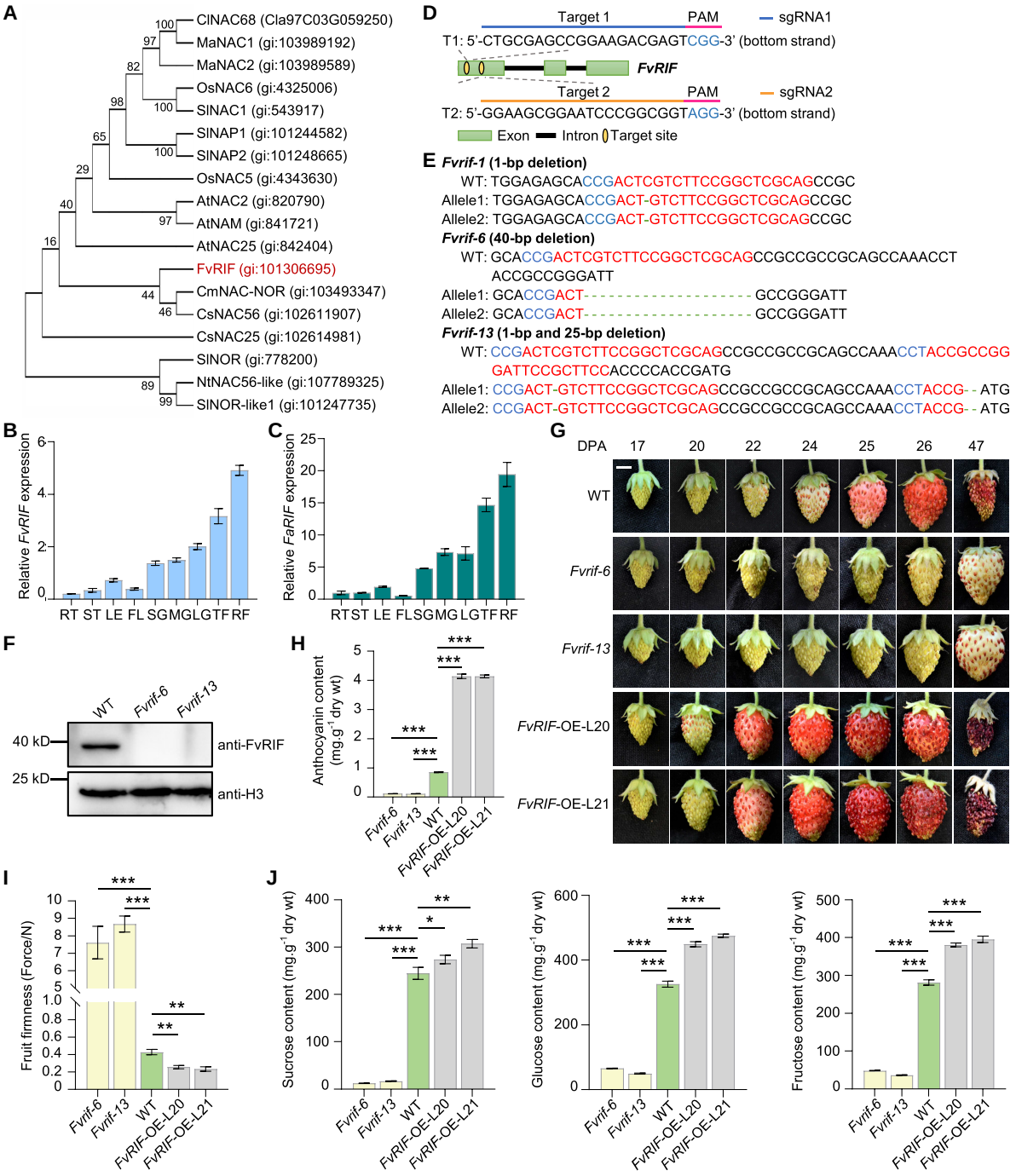

Figure 1. Mutation of *FvRIF* leads to the inhibition of strawberry fruit ripening. **A)** Phylogenetic analysis of FvRIF. The phylogenetic tree was generated by MEGA (version 10.1.8). Bootstrap values from 500 replicates for each branch are shown. At, *A. thaliana*; Cl, *C. lanatus*; Cm, *C. melo*; Cs, *C. sinensis*; Fv, *F. vesca*; Ma, *M. acuminata*; Nt, *N. tabacum*; Os, *Oryza sativa*; Sl, *S. lycopersicum*. **B), C)** Expression pattern of *RIF* in diploid strawberry (*FvRIF*, **B**) and octoploid strawberry (*FaRIF*, **C**) as determined by RT-qPCR. FL, flower; LE, leaf; RT, root; ST, stem. Values are means ± standard error of mean (SEM) from 3 biological replicates using *ACTIN* (FvH4_6g22300) as an internal control. **D)** Diagram of the sgRNAs with different target sequences (T1 and T2) designed to specifically target exon 1 of *FvRIF*. **E)** Genotyping of mutations mediated by CRISPR/Cas9 gene editing in the *Fvrif-1*, *Fvrif-6*, and *Fvrif-13* mutant lines. Red letters, sgRNA targets; Green dashed lines, edited sites; Blue letters, protospacer adjacent motif (PAM). The transgenic plants in the second generation were genotyped by Sanger sequencing of the genomic regions flanking the target sites. **F)** Absence of FvRIF protein in the *Fvrif-6* and *Fvrif-13* lines. Nuclear proteins were extracted from wild-type (WT) and mutant fruits at 28 DPA and subjected to immunoblot analysis using an anti-FvRIF antibody. Histone H3 was used as the internal control. **G)** Phenotypes of strawberry fruits from WT, *Fvrif* mutants or *FvRIF* overexpression lines. Scale bar, 0.5 cm. **H) to J)** Changes in anthocyanin contents **H)**, fruit firmness **I)**, and sugar contents **J)** in the mutants and overexpression lines at 28 DPA. Values are means ± SEM from 3 biological replicates. Statistical significance was determined by Student's *t*-test (*$P < 0.05$, **$P < 0.01$, ***$P < 0.001$).

Together, our data support the notion that FvRIF functions as a global regulator in the control of different ripening-related responses in strawberry fruit.

Genome-wide identification of FvRIF binding sites

To better understand FvRIF-mediated transcriptional regulation of fruit ripening, we performed DAP-seq to unravel FvRIF binding sites at the genome scale. DAP-seq has been recently employed to capture genome-wide DNA binding sites of TFs in their native sequence context (O'Malley et al. 2016; Galli et al. 2018; Wu et al. 2020; Nishida et al. 2021). For DAP-seq analysis, we used recombinant FvRIF fused to the HaloTag sequence to purify sheared genomic DNA from strawberry fruits. We prepared 2 independent biological replicates for DAP-seq and DNA "input" negative control libraries and analyzed them by high-throughput sequencing. The numbers of total clean sequencing reads and mapping rate for each replicate are shown in Supplemental Table S1. We consistently detected a total of 9,902 enriched peaks, corresponding to 7,899 genes, in both biological replicates (Fig. 2A; Supplemental Data Sets S1 to S3), which were thus considered as high-confidence FvRIF binding regions. The width of the binding sites ranged from 240 to 1,500 bp (Supplemental Fig. S7A), and the binding sites were highly centered on transcriptional start sites (TSS) (Fig. 2B). A detailed analysis of the binding profiles revealed that, although FvRIF bound to 5′ UTRs (4.4% of the binding sites), 3′ UTRs (5.0%), exons (14.8%), introns (12.5%), and intergenic regions (26.4%) (Fig. 2C), most binding sites (37.0%) were located within promoter regions (up to 2-kb upstream from a TSS) (Fig. 2C; Supplemental Data Set S4), which is consistent with FvRIF being a TF with DNA-binding ability and gene regulatory activity. Moreover, the binding sites of FvRIF were distributed evenly across the length of all 7 *F. vesca* chromosomes, suggesting that FvRIF shows no preference for a specific chromosome (Supplemental Fig. S7B).

To gain more insight into the DNA-binding properties of FvRIF, we conducted a de novo motif prediction based on the FvRIF-bound regions identified in our DAP-seq data using the Homer (version 3) tools, allowing the identification of 4 enriched motifs. The most enriched motif was represented by TACGTACGTAAC, which accounted for 4,649 FvRIF binding peaks (Fig. 2D). It is worth noting that the nucleotide sequence of this motif is derived from the core sequence CGT[G/A], a previously reported NAC recognition motif (Simpson et al. 2003; Ernst et al. 2004), confirming the reliability of our DAP-seq data. The flanking bases may determine the binding specificity and fine-tune the affinity of FvRIF. We identified 3 other motifs, TAGCTA(A/G)C, CTTC(A/G)TTT, and AGAAAGAA, which were present in 4,473, 3,500, and 2,222 FvRIF binding peaks, respectively (Fig. 2D).

Gene ontology (GO) enrichment analysis of the genes that contained FvRIF binding sites revealed a significant overrepresentation ($P < 0.05$; hypergeometric test) of categories such as "regulation of transcription," "phytohormone-mediated signaling pathway," "regulation of cell-wall organization or biogenesis," and "developmental maturation" (Fig. 2E), indicating that FvRIF may directly control multiple biological pathways relevant to fruit ripening.

Identification of FvRIF-regulated genes by transcriptome analysis

To identify genes that are transcriptionally regulated by FvRIF during fruit ripening, we performed comparative transcriptome analysis through transcriptome deep sequencing (RNA-seq) using fruits from 3 independent biological replicates of the wild type and mutants (*Fvrif-6* and *Fvrif-13*) at 28 DPA. In total, we obtained 405 million reads after trimming, 97.0% of which mapped to unique loci in the reference genome. A bioinformatic analysis identified 8,138 differentially expressed genes (DEGs), with 3,365 downregulated (Log_2(fold-change [FC]) < -1; false discovery rate [FDR] $<$ 0.05) and 4,773 upregulated ($Log_2(FC) > 1$; FDR < 0.05) genes in the *Fvrif-6* line relative to wild type (Fig. 3A; Supplemental Data Set S5). Similarly, 3,299 downregulated ($Log_2(FC) < -1$; FDR < 0.05) and 4,683 upregulated genes ($Log_2(FC) > 1$; FDR < 0.05) were differentially expressed in the *Fvrif-13* line (Fig. 3B; Supplemental Data Set S6). The overlap between the DEGs identified from each mutant defined 2,747 downregulated and 3,959 upregulated DEGs (Fig. 3, C and D; Supplemental Data Set S7). We obtained a high Pearson's correlation coefficient by comparing the transcriptomes of the 2 mutant lines, confirming their high transcriptional similarity (Supplemental Fig. S8). Notably, *FvRIF* mRNA levels were significantly lower in both lines compared to wild type (Supplemental Fig. S9, A and B), suggesting that genome editing might cause RNA instability due to frameshift mutations.

Next, we performed a GO enrichment analysis to identify biological processes enriched among the DEGs. This analysis revealed enrichment for processes such as "regulation of ABA-activated signaling pathway," "regulation of secondary metabolic process," and "glucose metabolic process" (Fig. 3E), supporting a function for FvRIF in the control of fruit development and ripening. Interestingly, some well-known ripening-related genes, e.g. *FvCHS1*-encoding chalcone synthase (CHS), involved in flavonoid biosynthesis (Hoffmann et al. 2006; Nakayama et al. 2019), *FvPL2*-encoding pectate lyase (PL), responsible for cell-wall disassembly (Jimenez-Bermudez et al. 2002), and *FvNCED5*-encoding 9-*cis*-epoxycarotenoid dioxygenase, implicated in ABA biosynthesis (Ji et al. 2012), exhibited altered mRNA levels in the *Fvrif* lines (Supplemental Fig. S10).

Determination of FvRIF-regulated direct target genes

We next sought to determine the FvRIF-regulated direct target genes by comparing the 7,899 FvRIF binding genes identified in our DAP-seq analysis with the 6,706 DEGs in the RNA-seq analysis of the *Fvrif* lines. We identified 2,080 genes in common between the DAP-seq and RNA-seq analyses, suggesting they are direct targets of FvRIF (Fig. 4A; Supplemental Data Set S8). Among them, 769 genes (37.0%) represented targets positively

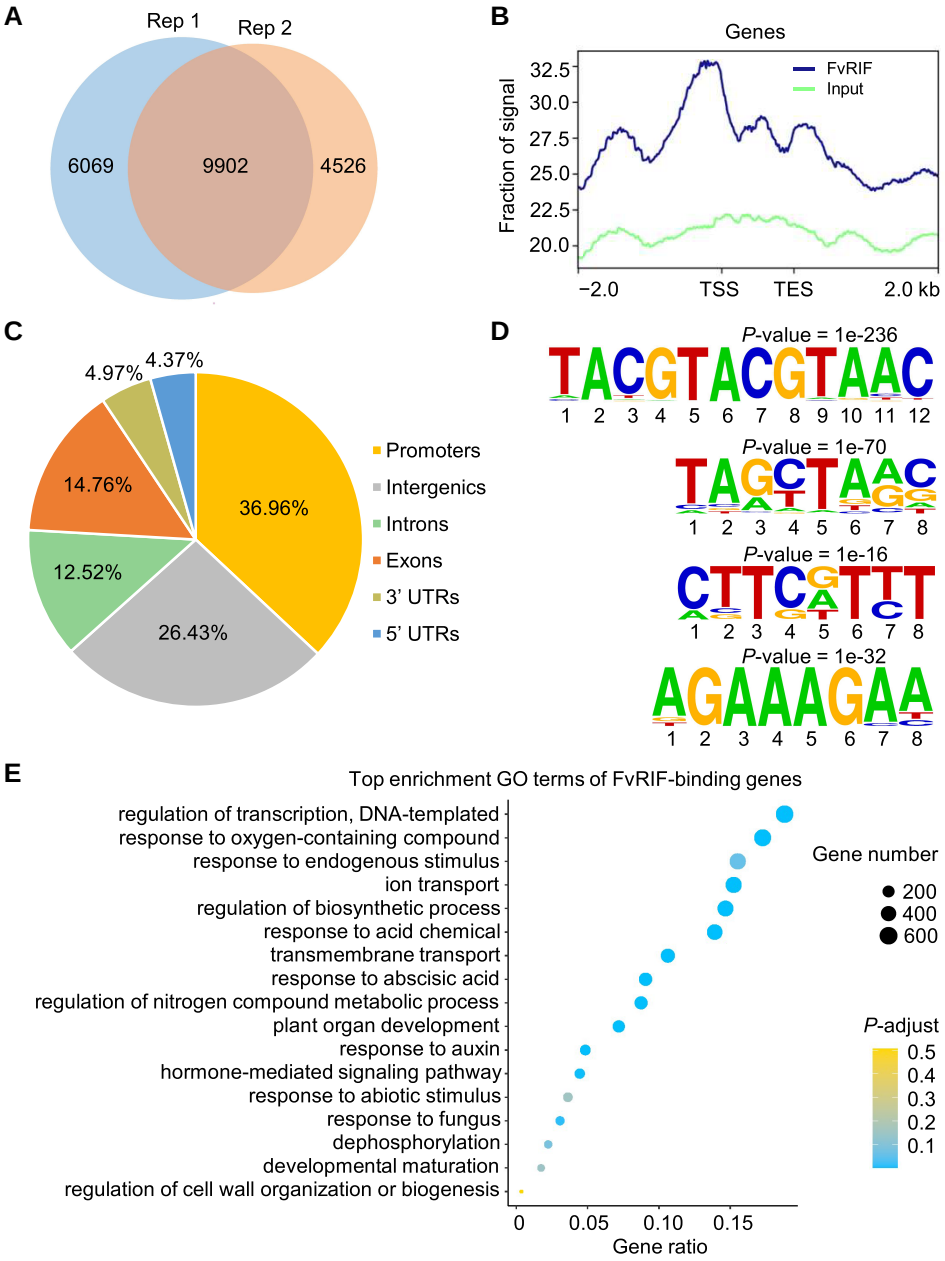

Figure 2. Genome-wide identification of FvRIF binding sites through DAP-seq. **A)** DAP-seq using 2 biological replicates reveals 9,902 high-confidence FvRIF binding peaks. **B)** Metaplot of FvRIF binding sites. The FvRIF binding sites are centered on the TSS. TES, transcription end site. **C)** Distribution of FvRIF binding peaks across genomic features. **D)** DNA logos of enriched DNA binding sites for FvRIF as determined by Homer (version 3). The *P*-values are shown. **E)** Top enriched GO terms of FvRIF-bound genes determined by DAP-seq. Bigger dots indicate more genes.

regulated by FvRIF, since they were downregulated in the *Fvrif* lines, while 1,311 genes (63.0%) were considered as targets negatively regulated by FvRIF, as they were upregulated in the *Fvrif* mutant lines (Fig. 4A; Supplemental Data Set S8). Kyoto Encyclopedia of Genes and Genomes (KEGG) pathway enrichment analysis showed that FvRIF-regulated direct target genes are involved in multiple metabolic pathways, including "plant hormone signal transduction," "starch and sucrose metabolism," "phenylpropanoid biosynthesis," and "flavonoid biosynthesis" (Fig. 4B).

Consistent with the function of FvRIF in the control of fruit ripening, we identified multiple genes associated with anthocyanin biosynthesis, cell-wall degradation, sugar metabolism, and aroma compounds generation as direct target genes of FvRIF (Fig. 4, C to F; Supplemental Table S2). Moreover, FaPYR2 (pyrabactin resistance 2), an ABA receptor, was also among the FvRIF-regulated direct target genes (Supplemental Data Set S8). The expression of *FvRIF* was induced by ABA (Supplemental Fig. S11), indicating that FvRIF may regulate the ABA pathway via a positive feedback loop. Interestingly, a

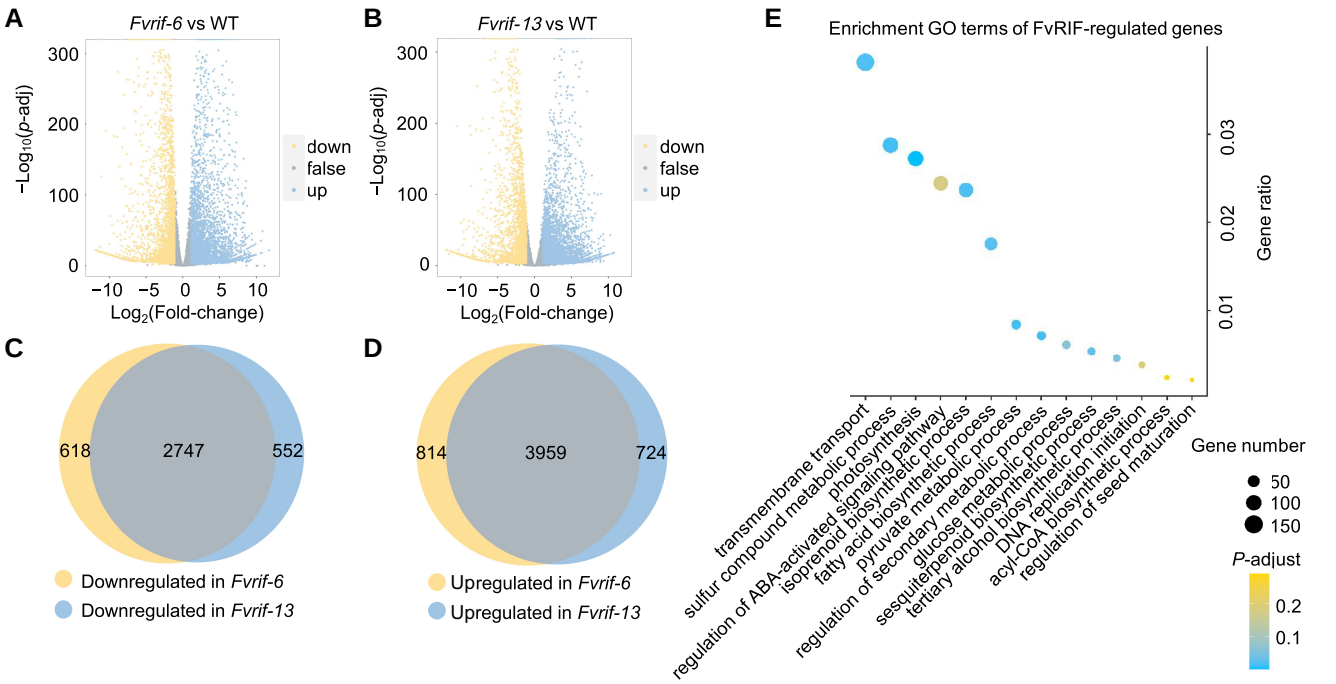

Figure 3. Transcriptome-based determination of FvRIF-regulated genes. **A), B)** Volcano plots revealing the DEGs in fruits of *Fvrif-6* **A)** and *Fvrif-13* **B)** mutant lines compared to wild type (WT) at 28 DPA by RNA-seq. Down, downregulated; Up, upregulated. Genes with more than two-fold changes in expression and FDR < 0.05 were considered as DEGs. **C), D)** Venn diagrams showing the overlapping downregulated **C)** and upregulated **D)** genes, respectively, in fruits of the 2 mutant lines (*Fvrif-6* and *Fvrif-13*). **E)** Top enriched GO terms of FvRIF-regulated genes as defined by RNA-seq analysis. Bigger dots indicate more gene numbers.

large number of the FvRIF target genes (137, 6.6%) encoded TFs (Supplemental Data Set S9), including ripening-related regulators such as *FvMYB10* (Medina-Puche et al. 2014; Castillejo et al. 2020), *FvSEP3* (*Sepallata 3*) (Pi et al. 2021), and *FvARF2* (*auxin-response factor 2*) (Yi et al. 2022) (Supplemental Table S2), suggesting that, besides the direct regulation of structural genes, FvRIF may indirectly regulate ripening by targeting important TF genes.

FvRIF directly regulates key genes in the anthocyanin biosynthetic pathway

Anthocyanins are the main pigments in strawberry fruits, which are biosynthesized by a series of enzymes including phenylalanine ammonia-lyase (PAL), CHS, chalcone–flavanone isomerase (CHI), flavanone 3-hydroxylase (F3H), dihydroflavonol 4-reductase (DFR), and leucoanthocyanidin dioxygenase/anthocyanidin synthase (ANS) (Castillejo et al. 2020). Interestingly, 6 genes in the anthocyanin biosynthetic pathway were direct FvRIF-regulated targets (Fig. 4C; Supplemental Data Set S8), which is consistent with the dramatic decrease in the anthocyanin content of *Fvrif* fruits compared to that in the wild type (Fig. 1H) and supports a direct role for FvRIF in this pathway. We thus selected 4 genes, i.e. *FvCHS1*, *FvDFR*, *FvANS*, and *FvUFGT*, which showed enriched binding sites in their promoter regions in the DAP-seq analysis (Fig. 5A), to validate the direct modulation of the anthocyanin biosynthetic pathway by FvRIF through these genes. To this end, we cloned the coding sequence of *FvRIF* and specific promoter fragments (200 bp) for these target genes into the pGADT7 (activation domain [AD]) and pAbAi vectors, respectively, which we then transformed in pairs into yeast (*Saccharomyces cerevisiae*) to perform a yeast 1-hybrid (Y1H) assay. As shown in Fig. 5B, only the yeast cells transformed with the vectors pGADT7-*FvRIF* and pAbAi containing promoter regions of the target genes (pAbAi-*proFvCHS1*, *proFvDFR*, *proFvANS*, and *proFvUFGT*), but not the negative control, survived on selective medium containing aureobasidin A (AbA; 100 ng/mL), indicating that FvRIF interacts with the promoters of *FvCHS1*, *FvDFR*, *FvANS*, and *FvUFGT* in yeast.

Furthermore, we performed an electrophoretic mobility shift assay (EMSA) with purified recombinant FvRIF to confirm that FvRIF interacts with the promoter fragments of each of these 4 anthocyanin-related genes. We observed a band shift for each promoter fragment when purified FvRIF was mixed with the biotin-labeled DNA probe harboring the binding motifs identified in our DAP-seq analysis (Fig. 5C), suggesting that FvRIF binds to the biotin-labeled promoter fragments. The shifted band was effectively competed by the addition of excess unlabeled DNA probe with intact binding motifs, but not by a probe with mutated binding motifs (Fig. 5C). These results indicate that FvRIF binds specifically to the promoters of *FvCHS1*, *FvDFR*, *FvANS*, and *FvUFGT* in vitro.

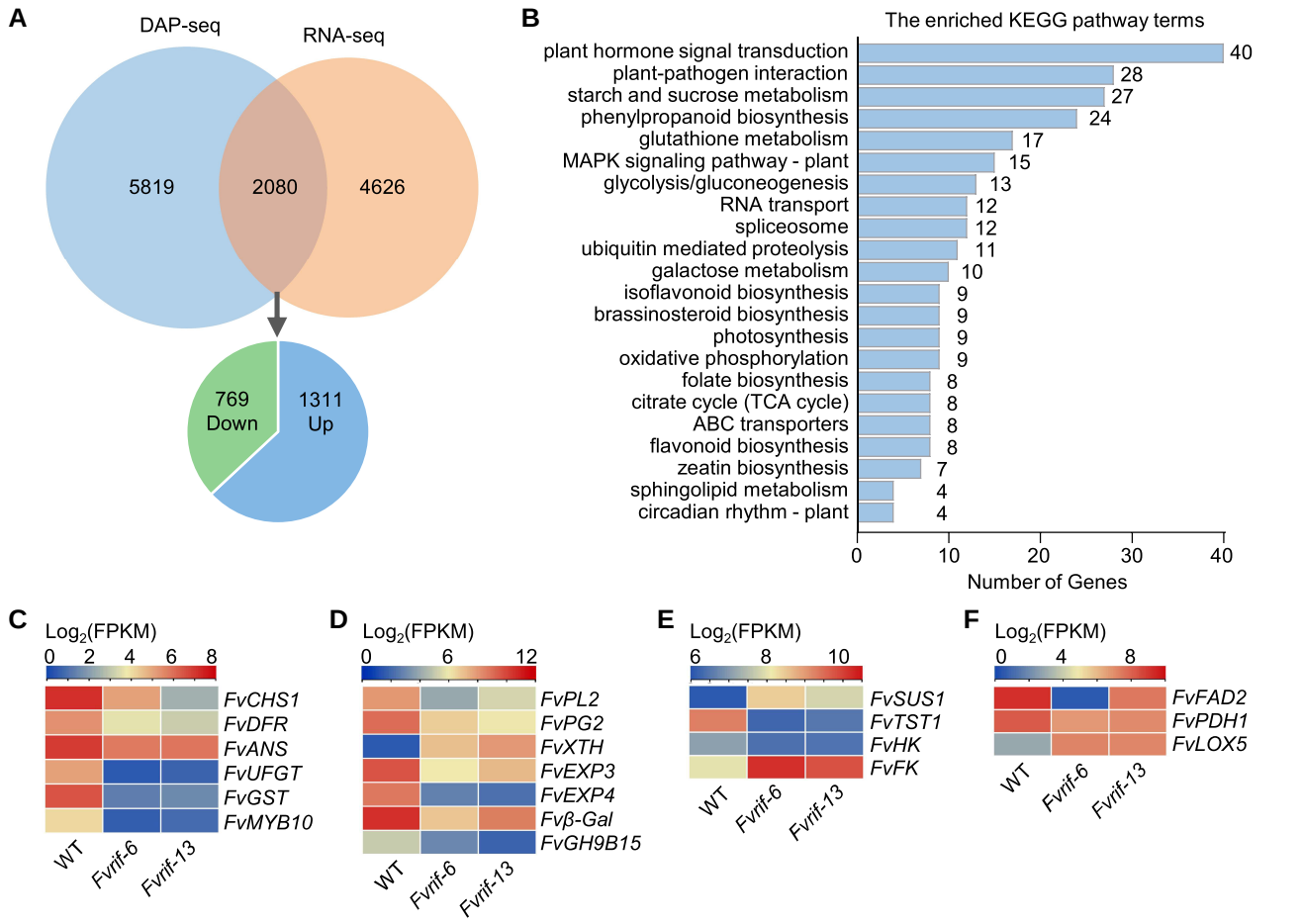

Figure 4. Identification of direct FvRIF-regulated target genes. **A)** Venn diagram showing the overlap between FvRIF-bound genes as revealed by DAP-seq and FvRIF-regulated genes identified by RNA-seq. The numbers of downregulated and upregulated FvRIF direct genes are indicated. **B)** Top KEGG-enriched terms for the direct FvRIF-regulated target genes. **C) to F)** Heatmap showing the expression of direct FvRIF-regulated target genes related to anthocyanin biosynthesis **C)**, cell-wall degradation **D)**, sugar metabolism **E)**, and aroma compounds generation **F)**. The expression of these genes revealed by RNA-seq in fruits of the mutant lines (*Fvrif-6* and *Fvrif-13*) and the wild type (WT) is shown. The detailed information is shown in Supplemental Data Set S7.

Finally, to assess whether FvRIF directly binds to these selected promoters in vivo, we performed a chromatin immunoprecipitation (ChIP) assay. For this purpose, we sonicated the chromatin to shear the genomic DNA to an average size of 250 to 1,500 bp (Supplemental Fig. S12A), followed by immunoprecipitation with affinity-purified anti-FvRIF polyclonal antibody, which specifically recognized FvRIF (Supplemental Fig. S12B), to capture the cross-linked DNA–protein complexes. The eluted DNA was then purified and subjected to qPCR analysis using specific primers (Supplemental Table S3) designed to amplify promoter sequences surrounding the binding motifs identified in our DAP-seq analysis. As shown in Fig. 5D, we observed specific enrichment for the promoter regions of *FvCHS1*, *FvDFR*, *FvANS*, and *FvUFGT* in FvRIF-bound chromatin, indicating that FvRIF binds to the promoter of these genes in vivo. These results validate the reliability of DAP-seq for identifying FvRIF-bound genes.

RNA-seq analysis showed that, compared to the wild type, the expression of *FvCHS1*, *FvDFR*, *FvANS*, and *FvUFGT* decreases significantly in fruits of the *Fvrif-6* and *Fvrif-13* mutant lines (Fig. 5E). RT-qPCR analysis confirmed the RNA-seq results (Fig. 5F), indicating that FvRIF positively regulates the expression of these structural genes. Collectively, our data show that FvRIF functions as a critical positive transcriptional regulator governing anthocyanin biosynthesis in strawberry fruits.

FvRIF directly modulates core genes involved in fruit softening

Fruit softening, which is catalyzed by a set of cell-wall degrading enzymes, represents 1 of the most significant characteristics in fruit ripening (Wang et al. 2018). Notably, our DAP-seq coupled with RNA-seq analysis identified 7 genes involved in fruit softening as direct FvRIF-regulated targets (Fig. 4D; Supplemental Data Set S8). We selected 4 of these genes for validation: the PL gene *FvPL2*, the polygalacturonase (PG) gene *FvPG2*, the xyloglucan endotransglucosylase/hydrolase gene *FvXTH*, and the expansin (EXP) gene *FvEXP3*. All 4 genes displayed enrichment

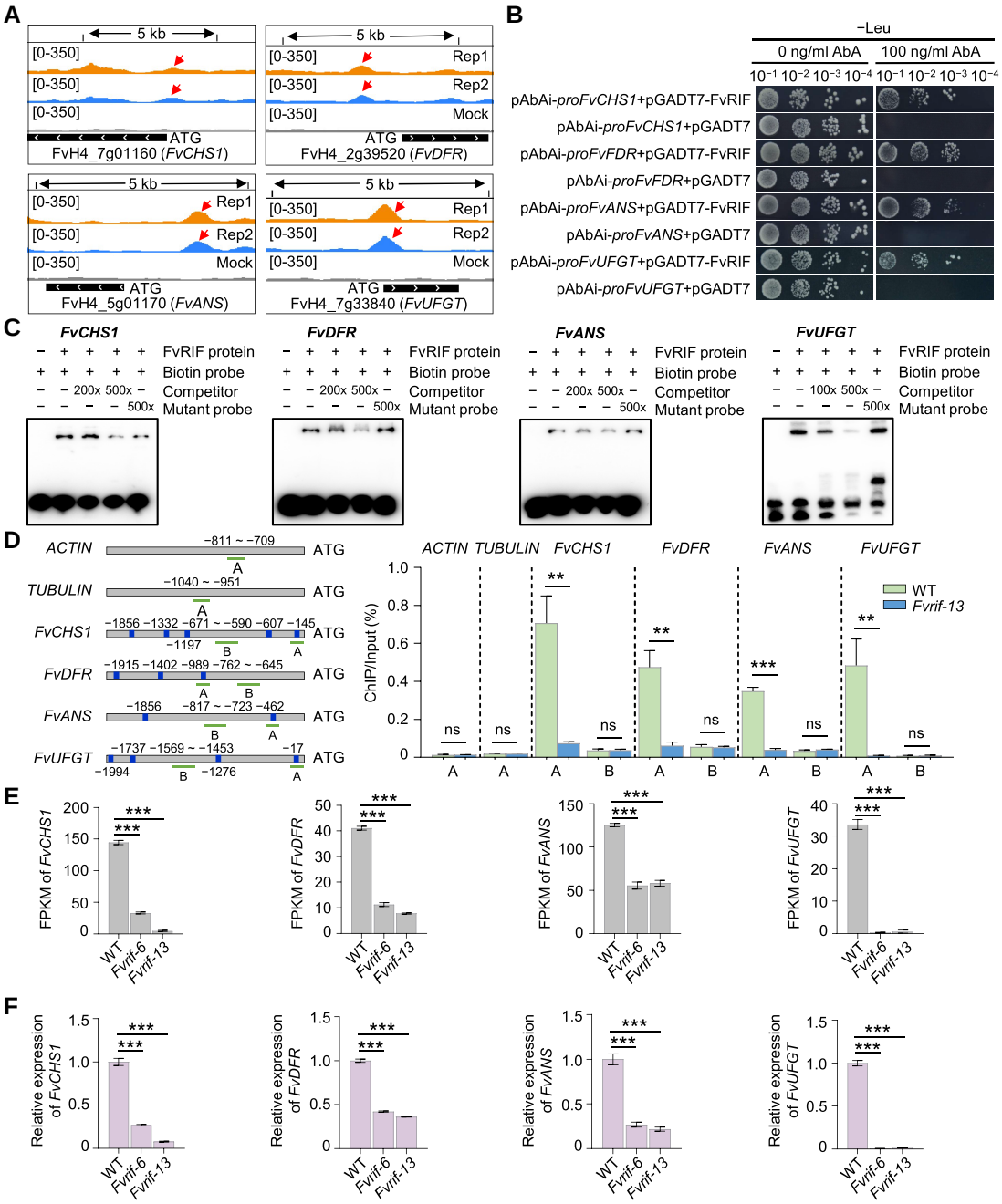

Figure 5. FvRIF-mediated direct regulation of genes responsible for anthocyanin biosynthesis in strawberry. **A)** FvRIF binding peaks (Repeats 1 and 2) and negative control (mock) over the *FvCHS1*, *FvDFR*, *FvANS*, and *FvUFGT* loci as determined by DAP-seq. [0 to 350] represents the scale of binding intensity as reflected by the height of the peak. UFGT, UDP-glucose flavonoid glucosyl-transferase. **B)** Y1H assay revealing the binding of FvRIF to the indicated promoter fragments. pGADT7-*FvRIF* served as the prey and pAbAi-*proFvCHS1*, *proFvDFR*, *proFvANS*, and *proFvUFGT* were used as the baits. The empty pGADT7 served as the negative control. The transformants were selected on SD/−Leu medium with AbA. **C)** EMSA shows that FvRIF directly binds to sequence motifs in the *FvCHS1*, *FvDFR*, *FvANS*, and *FvUFGT* promoters. Recombinant purified FvRIF (0.8 μg) was incubated with biotin-labeled probes (0.02 μM) or unlabeled DNA probe with intact (competitor) or mutated (mutant probe) FvRIF binding motifs. **D)** ChIP-qPCR assays reveal the direct binding of FvRIF to the promoters of the indicated genes. The promoter structures of the target genes are shown (left panel). Blue boxes, FvRIF binding motifs as identified by DAP-seq; Green lines, regions used for ChIP-qPCR. The numbers indicate the positions of these motifs relative to the ATG. Values are the percentage of DNA fragments coimmunoprecipitated with anti-FvRIF antibodies in fruits of wild type (WT) or the *Fvrif-13* mutant line relative to the input DNAs (right panel). Negative controls (*ACTIN* and *TUBULIN*) are included. **E)** Expression of the indicated genes in fruits of *Fvrif* lines (*Fvrif-6* and *Fvrif-13*) and WT at 28 DPA by RNA-seq. **F)** Verification of gene expression by RT-qPCR. *ACTIN* was used as an internal control. For **D) to F)**, values are means ± SEM from 3 biological replicates. Asterisks indicate significant differences (**$P < 0.01$, ***$P < 0.001$; Student's *t*-test).

peaks in their promoter regions in the DAP-seq analysis (Fig. 6A), suggesting that they appear to be potential direct targets of FvRIF. Y1H analysis showed that FvRIF interacts with the promoters of the selected genes (Fig. 6B). Furthermore, EMSA and ChIP assay confirmed that FvRIF may directly bind to the promoters of these genes in vitro and in vivo (Fig. 6, C and D). When we analyzed the expression of these target genes in the RNA-seq data (Fig. 6E) and by RT-qPCR analysis (Fig. 6F), *FvPL2*, *FvPG2*, and *FvEXP3* showed a significant downregulation in fruits of the *Fvrif-6* and *Fvrif-13* mutant lines compared to the wild type, indicating that FvRIF positively regulates these genes. By contrast, *FvXTH* showed the opposite expression pattern (Fig. 6, E and F), which is consistent with its previously reported negative correlation with fruit softening (Paniagua et al. 2014). Together, these results demonstrate that FvRIF acts as a positive transcriptional regulator in controlling directly genes involved in strawberry fruit softening.

FvRIF directly regulates TF genes involved in fruit ripening

TFs are important regulators controlling strawberry fruit ripening (Sanchez-Gomez et al. 2022). We identified a total of 137 TF-encoding genes as direct targets of FvRIF, as revealed by our DAP-seq combined with RNA-seq (Supplemental Data Set S9). Only 4 of these TF genes, *FvMYB10*, *FvSEP3*, *FvSPT*, and *FvARF2*, have been previously reported to be involved in the regulation of strawberry ripening. FvMYB10 acts as a key positive regulator of anthocyanin biosynthesis (Lin-Wang et al. 2010; Castillejo et al. 2020), while FvSEP3, a MADS-box TF, and FvSPT (Spatula), a basic helix–loop–helix (bHLH) TF, are necessary for the regulation of fruit development and ripening (Tisza et al. 2010; Pi et al. 2021). By contrast, FvARF2 negatively regulates fruit ripening and quality (Yi et al. 2022). DAP-seq analysis revealed FvRIF binding peaks in the promoter regions of these 4 TF genes (Fig. 7A). We detected an interaction between FvRIF and the promoters of all 4 genes by Y1H analysis in yeast (Fig. 7B). We also performed EMSA and a ChIP assay, which supported the notion that FvRIF binds specifically to the promoters of these TF genes in vitro and in vivo (Fig. 7, C and D). Expression analyses by RNA-seq (Fig. 7E) and RT-qPCR (Fig. 7F) showed that *FvMYB10*, *FvSEP3*, and *FvSPT* exhibit decreased expression levels, whereas *FvARF2* display increased expression levels, in fruits of the mutant lines (*Fvrif-6* and *Fvrif-13*) relative to the wild type. These results suggest that FvRIF exerts its role in controlling fruit ripening in part by regulating the expression of TF genes known to be involved in ripening.

FvRIF physically interacts with FvMAPK6

As a classical posttranslational modification, protein phosphorylation regulates the activity of TFs (Zhang et al. 2018). We carried out a prediction analysis for phosphorylation sites in FvRIF by KinasePhos (http://kinasephos.mbc.nctu.edu.tw/predict.php). This analysis led to the prediction of Thr-310 as a putative phosphorylation site, whose cognate kinases appear to be MAPKs. Thus, we hypothesized that FvRIF may be subjected to MAPK-mediated phosphorylation. We performed a yeast 2-hybrid (Y2H) with the 12 MAPK proteins annotated in *F. vesca* (Zhou et al. 2017) against FvRIF, showing that FvRIF interacts with FvMAPK6, but not with any other MAPKs (Fig. 8A). We then performed split luciferase complementation imaging (LCI) assays, in which we transiently coexpressed *FvRIF-nLUC* and *cLUC-FvMAPK6* in leaves of *Nicotiana benthamiana*. We detected intense luciferase activity in *N. benthamiana* leaves coexpressing *FvRIF-nLUC* and *cLUC-FvMAPK6*, but not the negative controls (Fig. 8B), indicating that FvRIF interacts with FvMAPK6 in planta. We next set out to determine whether FvRIF interacts with FvMAPK6 in vitro by pull-down assay. We incubated recombinant glutathione S-transferase (GST)-tagged FvMAPK6 (GST-FvMAPK6) bound to glutathione Sepharose beads with maltose-binding protein (MBP)-tagged FvRIF (MBP-FvRIF) and detected the precipitated products by immunoblot analysis. As shown in Fig. 8C, MBP-FvRIF, but not MBP alone, could directly bind to GST-FvMAPK6 in vitro. Finally, to verify the interactions between FvRIF and FvMAPK6, we performed a coimmunoprecipitation (Co-IP) assay from protein extracts of *N. benthamiana* leaves coexpressing HA-tagged FvRIF (*HA-FvRIF*) and Flag-tagged FvMAPK6 (*FvMAPK6-Flag*). Indeed, HA-FvRIF was immunoprecipitated with FvMAPK6-Flag by anti-Flag beads, and FvMAPK6-Flag was immunoprecipitated with HA-FvRIF by anti-HA beads (Fig. 8D). Taken together, these data reveal that FvRIF interacts with FvMAPK6.

To examine the intracellular localization of FvMAPK6 and FvRIF, we individually cloned their coding sequences into a vector to generate a translational fusion with the red fluorescent protein mCherry or GFP at their C-terminus, respectively. Confocal laser scanning microscopy showed a fluorescent signal throughout the cell for FvMAPK6-mCherry, while we detected FvRIF-GFP in the nucleus (Fig. 8E). The fluorescent signals of FvRIF-GFP colocalized with those of FvMAPK6-mCherry in the nucleus, suggesting the subcellular colocalization of FvRIF and FvMAPK6, thus supporting their interaction in planta (Fig. 8E).

FvMAPK6 phosphorylates FvRIF at Thr-310

The observed physical interaction between FvRIF and FvMAPK6 proteins prompted us to investigate whether FvRIF was phosphorylated by FvMAPK6 using Phos-tag SDS–PAGE, an in vitro phosphorylation assay. We used the kinase FvMKK4, which was previously reported to function upstream of FvMAPK3 in strawberry, as a putative activator (Mao et al. 2022). As shown in Fig. 9A, without activation by the constitutively active variant FvMKK4^{DD}, FvMAPK6 was not able to phosphorylate FvRIF, suggesting the importance of phosphorylation-induced activation of FvMAPK6 by its upstream kinase FvMKK4. Importantly, the presence of FvMKK4^{DD} resulted in the phosphorylation of FvRIF (pFvRIF), as evidenced by a mobility shift in Phos-tag gels (Fig. 9A). Furthermore, the abundance of the phosphorylated form decreased in the presence of lambda phosphatase (λ-PPase) (Fig. 9B), confirming that the upper band was indeed

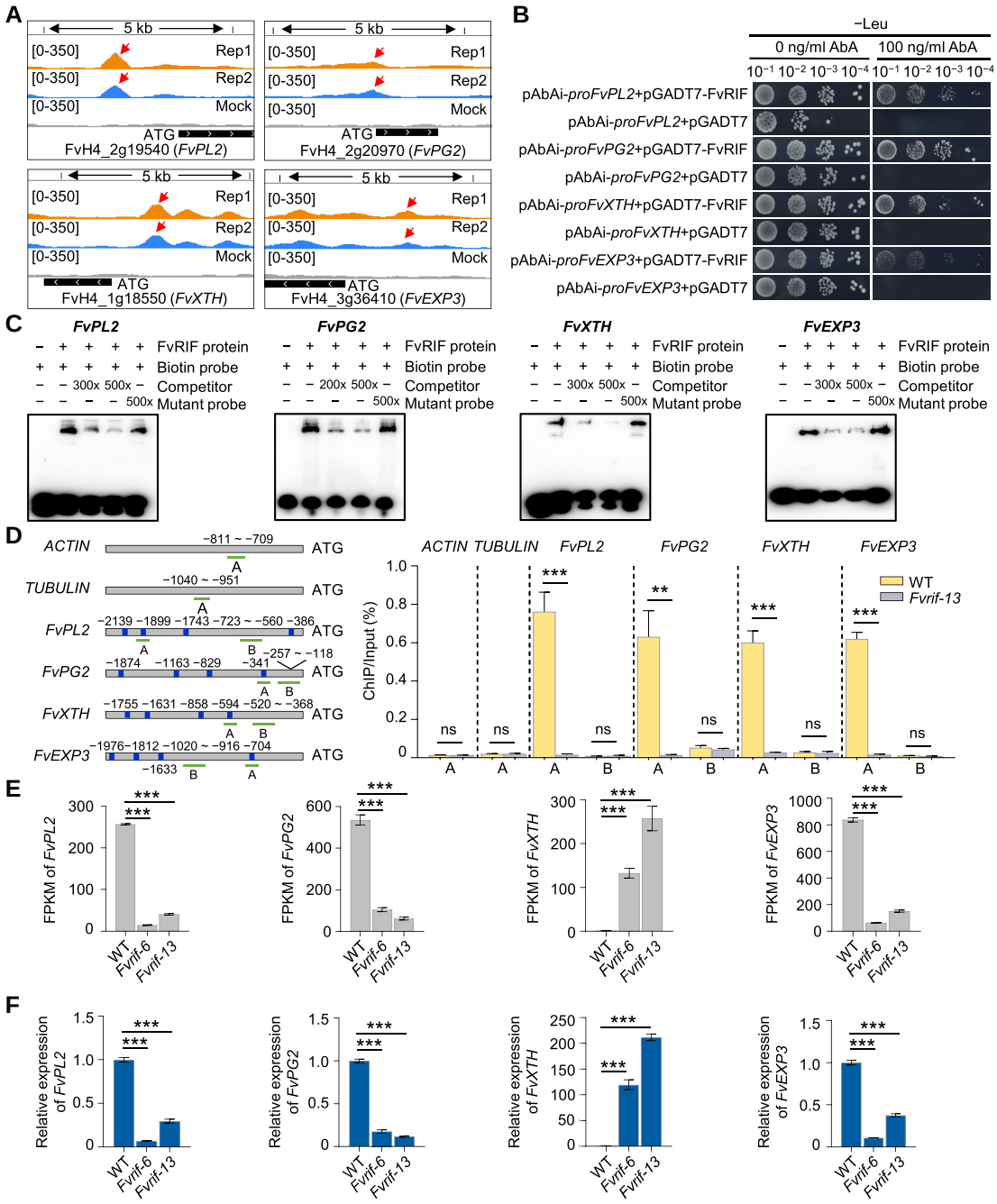

Figure 6. FvRIF-mediated direct regulation of genes involved in fruit softening. **A)** FvRIF binding peaks (Repeats 1 and 2) and negative control (mock) over the *FvPL2*, *FvPG2*, *FvXTH*, and *FvEXP3* loci as determined by DAP-seq. [0 to 350] represents the intensity of binding as reflected by the height of the peak. **B)** Y1H assay revealing the binding of FvRIF to the indicated promoter fragments. pGADT7-*FvRIF* served as the prey and the pAbAi-*proFvPL2*, *proFvPG2*, *proFvXTH*, and *proFvEXP3* were used as the baits. Empty pGADT7 served as the negative control. The transformants were selected on SD/−Leu medium with AbA. **C)** EMSA shows that FvRIF directly binds to sequence motifs in the *FvPL2*, *FvPG2*, *FvXTH*, and *FvEXP3* promoters. Recombinant purified FvRIF (0.8 μg) was incubated with biotin-labeled probes (0.02 μM) or unlabeled DNA probe with intact (competitor) or mutated (mutant probe) FvRIF binding motifs. **D)** ChIP-qPCR assays revealing the direct binding of FvRIF to the promoters of the indicated genes. The promoter structures of the target genes are shown (left panel). Blue boxes, FvRIF binding motifs as identified by DAP-seq; Green lines, regions used for ChIP-qPCR. The numbers indicate the positions of these motifs relative to the ATG. Values are the percentage of DNA fragments coimmunoprecipitated with anti-FvRIF antibodies in fruits of wild-type (WT) or the *Fvrif-13* mutant line relative to the input DNAs (right panel). Negative controls (*ACTIN* and *TUBULIN*) are included. **E)** Expression of the indicated genes in fruits of *Fvrif* lines (*Fvrif-6* and *Fvrif-13*) and WT at 28 DPA by RNA-seq. **F)** Verification of gene expression by RT-qPCR. *ACTIN* was used as an internal control. For **D) to F)**, values are means ± SEM from 3 biological replicates. Asterisks indicate significant differences (***$P < 0.001$; Student's *t*-test).

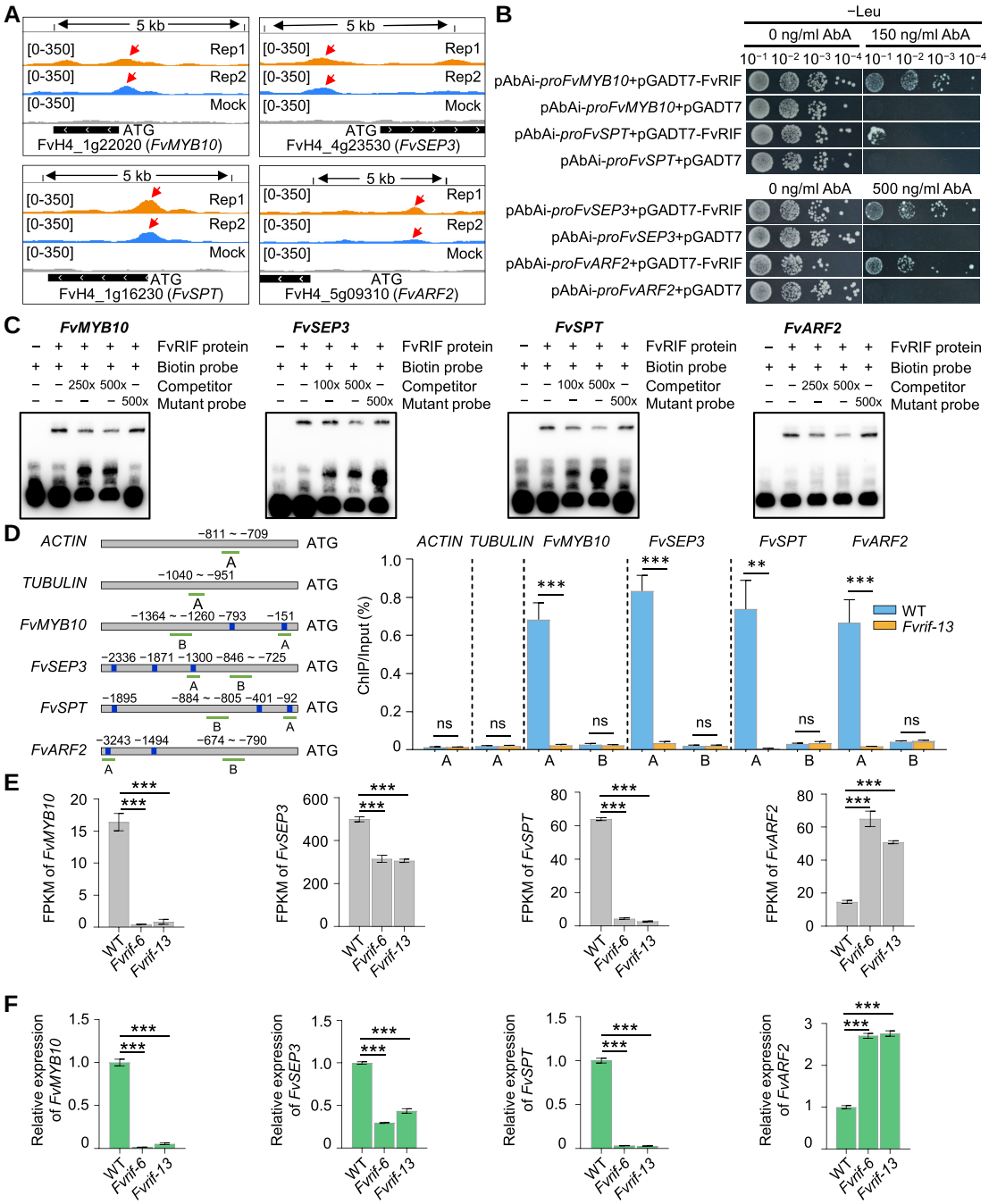

Figure 7. FvRIF-mediated direct regulation of TF genes involved in fruit ripening. **A)** FvRIF binding peaks (Repeats 1 and 2) and negative control (mock) over the *FvMYB10*, *FvSEP3*, *FvSPT*, and *FvARF2* loci as determined by DAP-seq. [0 to 350] represents the intensity of binding as reflected by the heights of the peak. **B)** Y1H assay revealing the binding of FvRIF to the indicated promoter fragments. pGADT7-*FvRIF* served as the prey and pAbAi-*proFvMYB10*, *proFvSEP3*, *proFvSPT*, and *proFvARF2* were used as the baits. Empty pGADT7 served as the negative control. The transformants were selected on SD/−Leu medium with AbA. **C)** EMSA shows that FvRIF directly binds to the motifs in the *FvMYB10*, *FvSEP3*, *FvSPT*, and *FvARF2* promoters. Recombinant purified FvRIF (0.8 μg) was incubated with biotin-labeled probes (0.02 μM) or unlabeled DNA probe with intact (competitor) or mutated (mutant probe) FvRIF binding motifs. **D)** ChIP-qPCR assays reveal the direct binding of FvRIF to the promoters of the indicated genes. The promoter structures of the target genes are shown (left panel). Blue boxes, FvRIF binding motifs as identified by DAP-seq; Green lines, regions used for ChIP-qPCR. The numbers indicate the positions of these motifs relative to the ATG. Values are the percentage of DNA fragments coimmunoprecipitated with anti-FvRIF antibodies in fruits of wild-type (WT) or the *Fvrif-13* mutant line relative to the input DNAs (right panel). Negative controls (*ACTIN* and *TUBULIN*) are included. **E)** Expression of the indicated genes in fruits of *Fvrif* lines (*Fvrif-6* and *Fvrif-13*) and WT at 28 DPA by RNA-seq. **F)** Verification of gene expression by RT-qPCR. *ACTIN* was used as an internal control. For **D) to F)**, values are means ± SEM from 3 biological replicates. Asterisks indicate significant differences (***$P < 0.001$; Student's *t*-test).

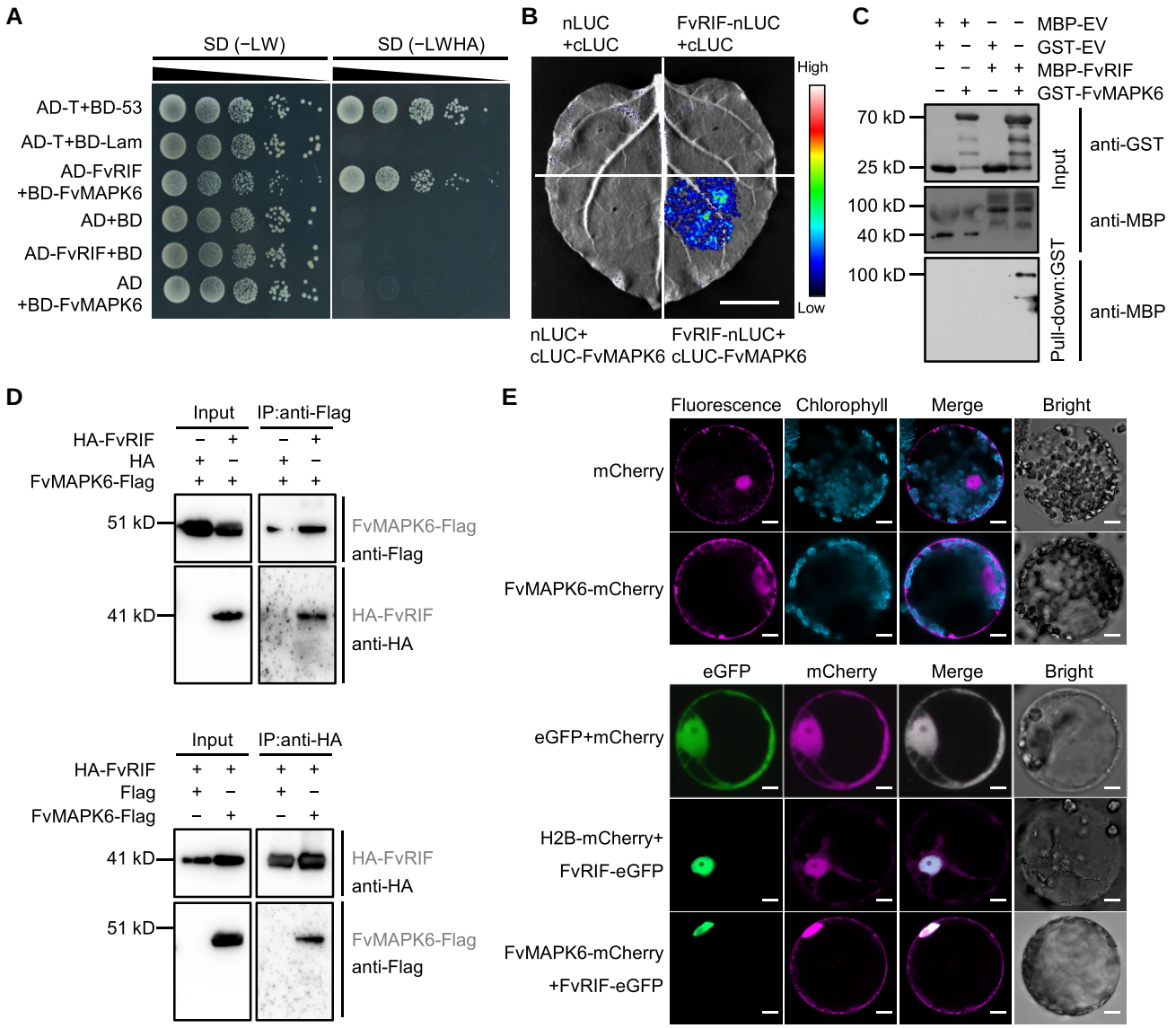

Figure 8. Interaction between FvRIF and FvMAPK6. **A)** Y2H assay revealing the interactions between FvRIF and FvMAPK6. FvMAPK6 fused to the BD of GAL4 (*BD-FvMAPK6*) and FvRIF fused to the AD of GAL4 (*AD-FvRIF*) were coexpressed in yeast. The transformants were selected on SD/−Leu/−Trp (−LW) medium and SD/−Leu/−Trp/−His/−Ade medium (−LWHA). The transformants carrying empty vectors (BD or AD) were used as negative controls. **B)** LCI assay revealing the interaction between FvRIF and FvMAPK6. FvMAPK6 fused to the C-terminus of LUC (*cLUC-FvMAPK6*) was coexpressed with FvRIF fused to the N-terminus of LUC (*FvRIF-nLUC*) in *N. benthamiana* leaves. Scale bar, 1 cm. **C)** FvRIF interacts with FvMAPK6 as determined by pull-down assay. Recombinant GST-FvMAPK6 bound to glutathione Sepharose beads was incubated with MBP-FvRIF. The eluted proteins were detected by immunoblotting using anti-GST and anti-MBP antibodies, respectively. GST-EV and MBP-EV served as negative control. **D)** Co-IP assay revealing the interaction between FvRIF and FvMAPK6. *FvMAPK6-Flag* and *HA-FvRIF* were coexpressed in *N. benthamiana* leaves. Total proteins were extracted from the infiltrated leaves and immunoprecipitated by anti-Flag or anti-HA magnetic beads. The eluted proteins were then detected by immunoblotting using anti-Flag and anti-HA antibodies, respectively. **E)** FvRIF colocalizes with FvMAPK6 in the nucleus. *Agrobacteria* carrying *35S:FvRIF-eGFP* and *35S:FvMAPK6-mCherry* constructs were transiently infiltrated in *N. benthamiana* leaves. *N. benthamiana* protoplasts coexpressing *eGFP* and *mCherry* were used as the negative control. *H2B-mCherry* serves as nucleus marker. Photographs of *N. benthamiana* protoplasts were taken 48-h postinfiltration under confocal microscopy. Scale bars, 10 μm.

phosphorylated FvRIF resulting from the activation by the FvMKK4–FvMAPK6 module.

We next aimed to identify the phosphorylation sites in FvRIF. For this purpose, we incubated recombinant FvRIF with $FvMKK4^{DD}$ and FvMAPK6 to induce phosphorylation. We then subjected phosphorylated FvRIF to liquid chromatography tandem MS (LC-MS/MS) analysis, leading to the identification of 5 high-confidence phosphorylation sites, Tyr-271, Ser-283, Ser-294, Ser-299, and Thr-310 (Figs. 9C and S13). A site-directed mutagenesis analysis showed that mutation of all 5 phosphorylation sites ($FvRIF^{5A}$) dramatically reduces FvMAPK6-dependent pFvRIF (Fig. 9D).

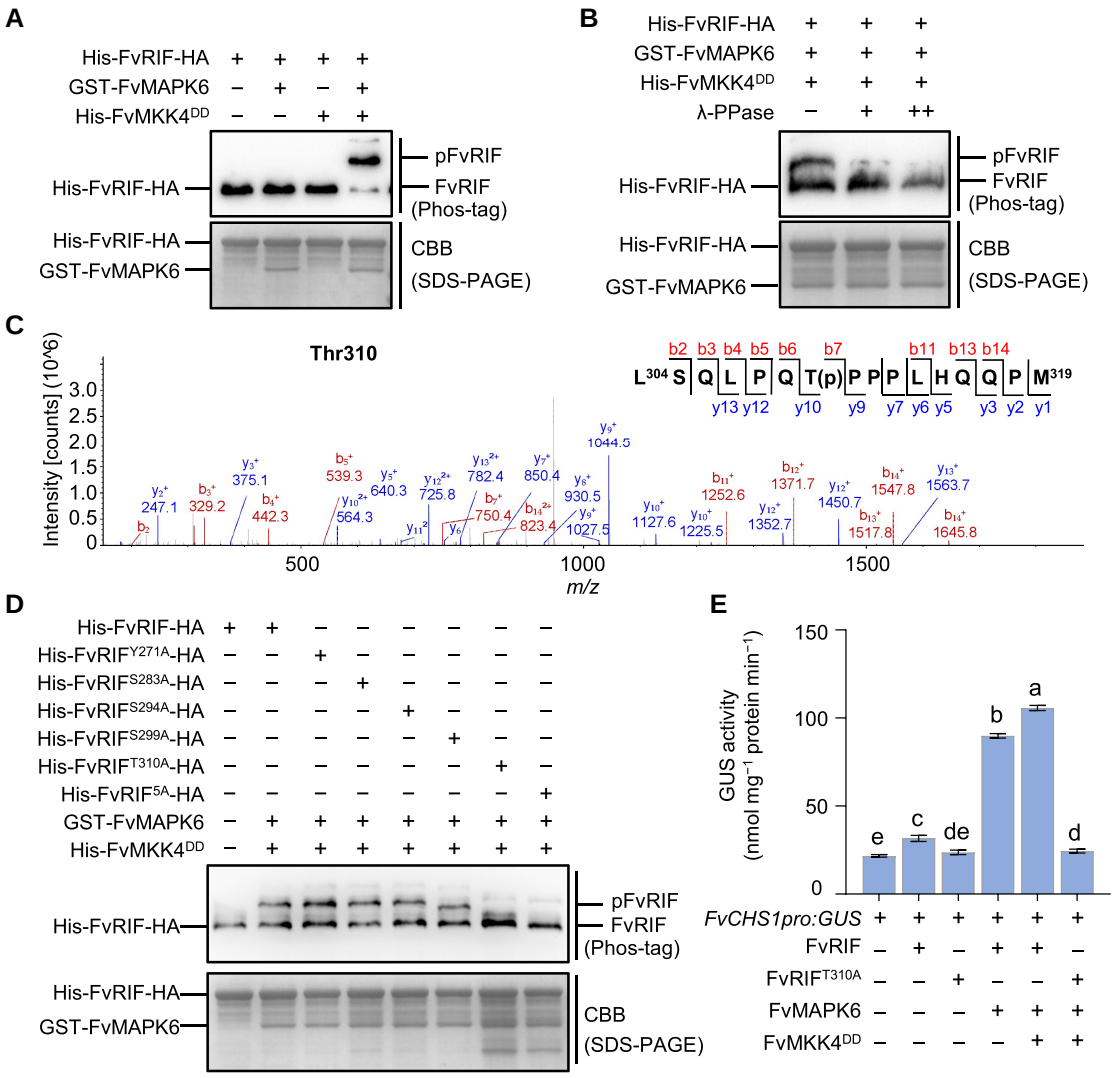

Figure 9. FvMAPK6-mediated FvRIF phosphorylation occurs at Thr-310. **A)** In vitro phosphorylation assay. Recombinant His-FvRIF-HA, GST-FvMAPK6, and His-FvMKK4^{DD} were incubated in kinase buffer and detected for phosphorylation by Phos-tag SDS–PAGE. Immunoblotting was conducted using an anti-HA antibody. CBB staining (bottom) indicates uniform sample loading. **B)** pFvRIF is diminished after treatment with lambda phosphatase (λ-PPase), often used to dephosphorylate substrates. **C)** Identification of FvRIF sites phosphorylated by FvMAPK6 via LC-MS/MS. The mass spectrum of peptide with phosphorylation sites at the Thr-310 residue is shown. The b-ions and y-ions and the corresponding peptide sequence are presented, with phosphorylated threonine (T) residue marked by (p). **D)** Phosphorylation analysis of FvRIF and its variant forms FvRIF^{Y271A}, FvRIF^{S283A}, FvRIF^{S294A}, FvRIF^{S299A}, FvRIF^{T310A}, and FvRIF^{5A}. Recombinant His-FvMKK4^{DD}, GST-FvMAPK6, and His-FvRIF-HA or its variant forms were mixed in kinase reaction buffer and detected for phosphorylation by Phos-tag SDS–PAGE. **E)** Determination of FvRIF transcriptional activation activity. *FvMKK4* ^{DD}, *FvMAPK6*, and *FvRIF* or its variant form *FvRIF*^{T310A} were used as effector constructs and cotransformed into LG strawberry fruits with the *FvCHS1pro:GUS* reporter. Data are the means ± SEM from 3 replicates. Data are analyzed using ANOVA. Different lowercase letters indicate significant differences according to Tukey's test ($P < 0.05$).

Further analysis showed that only FvRIF^{T310A} (substitution of Thr-310 by alanine [A]) exhibits a significant decrease in FvMAPK6-induced FvRIF phosphorylation, whereas FvRIF^{Y271A}, FvRIF^{S283A}, FvRIF^{S294A}, and FvRIF^{S299A} displayed little effect (Fig. 9D), indicating that Thr-310 serves as the key site responsible for FvMAPK6-mediated pFvRIF.

Finally, to determine whether the transcriptional activity of FvRIF is regulated by its phosphorylation status, we conducted a *GUS* transcriptional activity assay. We thus placed *GUS* under the control of the *FvCHS1* promoter, a direct FvRIF-regulated target, as described in Fig. 5. As shown in Fig. 9E, FvRIF activated the transcription of *GUS*. Remarkably, the FvMAPK6-dependent pFvRIF significantly increased *GUS* transcription, whereas the FvRIF^{T310A} variant completely abolished the *trans*-activation of the *FvCHS1pro:GUS* reporter (Fig. 9E). Together, these data suggest that pFvRIF at Thr-310 by the FvMKK4–FvMAPK6 module is essential to positively regulate its activity.

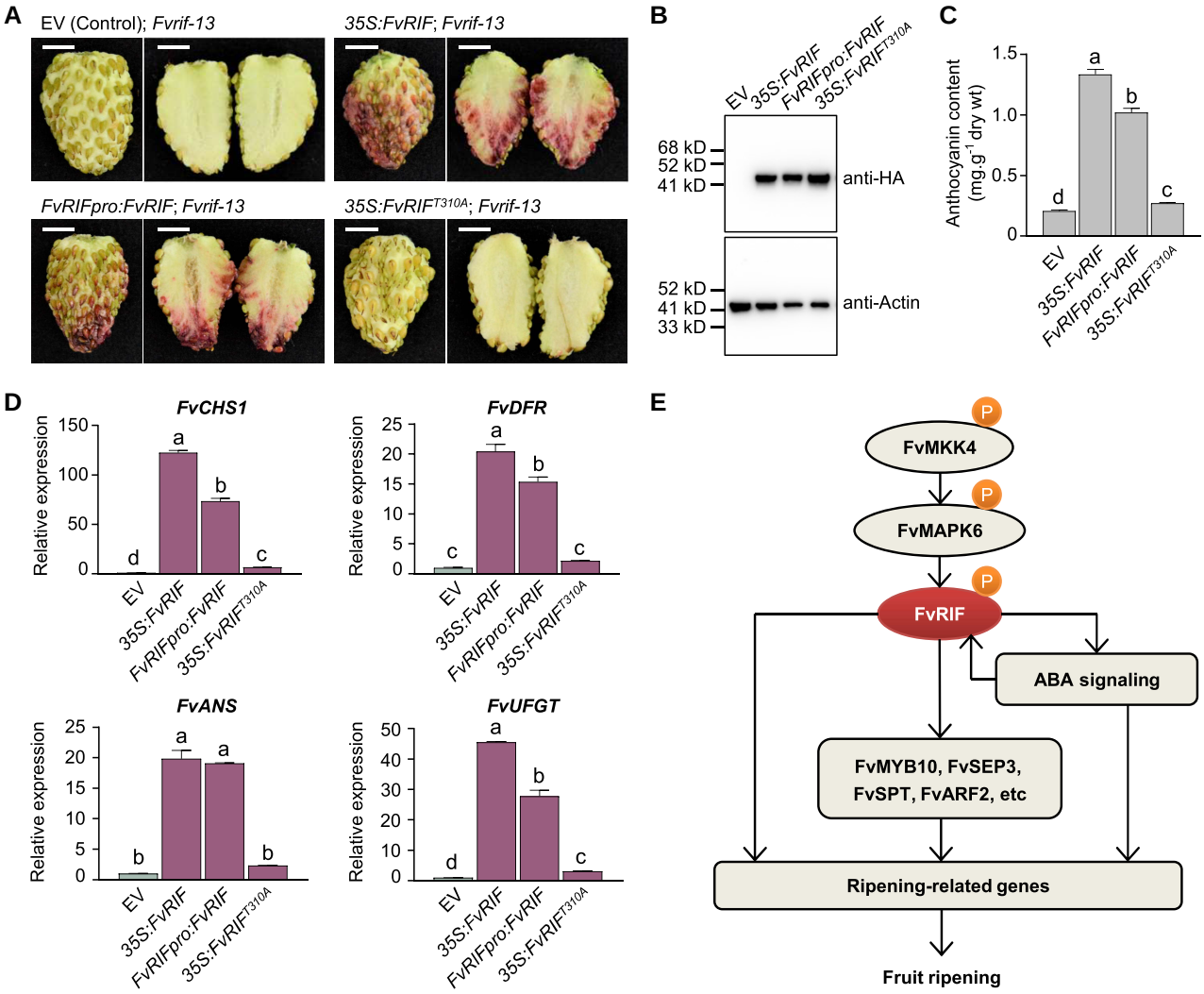

Figure 10. FvRIF phosphorylation is required for its activation in strawberry. **A)** Images showing the fruits of the *Fvrif-13* mutant transiently expressing *35S:FvRIF-HA*, *FvRIFpro:FvRIF-HA*, *35S:FvRIF^{T310A}-HA*, or empty vector (EV). In each case, 1 representative example is shown from at least 10 infiltrated fruits. Scale bars, 0.5 cm. **B)** Immunoblot assay revealing the efficiency of transient expression. Actin was used as a loading control. **C)** Anthocyanin contents in the fruits shown in **A)**. **D)** Expression levels of *FvCHS1*, *FvDFR*, *FvANS*, and *FvUFGT* in the fruits shown in **A)** as determined by RT-qPCR. *ACTIN* was used as an internal control. For **C)** and **D)**, values are means ± SEM from 3 biological replicates. Data are analyzed using ANOVA. Different lowercase letters indicate significant differences according to Tukey's test ($P < 0.05$). **E)** A proposed model for the regulation of fruit ripening by FvRIF in strawberry. Protein phosphorylation mediated by the FvMKK4–FvMAPK6 module activates the transcriptional activity of FvRIF, which directly regulates ripening-related genes to control fruit ripening. FvRIF also indirectly regulates ripening-related genes by targeting a number of TFs (e.g. FvMYB10, FvSEP3, FvSPT, and FvARF2) or the ABA pathway, which can promote *FvRIF* expression via a positive feedback loop.

Phosphorylation is indispensable for the activation of FvRIF in strawberry

To confirm that FvRIF phosphorylation regulates its activity in vivo, we took advantage of the *Fvrif* mutant lines. Accordingly, we transiently expressed various constructs in fruits of the *Fvrif-13* mutant: intact FvRIF (driven by the cauliflower mosaic virus [CaMV] 35S promoter or native promoter) or its mutated variant FvRIF^{T310A}, in which the key phosphorylation site (Thr-310) was mutated to A. As shown in Fig. 10A, intact FvRIF but not its mutated variant FvRIF^{T310A} rescued the ripening defect of the *Fvrif-13* mutant. Immunoblot analysis confirmed the successful accumulation of FvRIF and FvRIF^{T310A} (Fig. 10B). The anthocyanin content was significantly enhanced in fruits of the *Fvrif-13* mutant transiently expressing intact *FvRIF* (Fig. 10C), concomitant with an increase in expression levels of genes involved in anthocyanin biosynthesis, including *FvCHS1*, *FvDFR*, *FvANS*, and *FvUFGT* (Fig. 10D). By contrast, we observed little change in anthocyanin content or gene expression in fruits of the *Fvrif-13* mutant transiently expressing the mutant variant *FvRIF^{T310A}* (Fig. 10, C and D). These findings suggest that phosphorylation plays a critical role in the regulation of FvRIF activity in strawberry.

Based on our results presented in this study, we propose a model for FvRIF-mediated transcriptional regulation of fruit

ripening in strawberry (Fig. 10E). During strawberry fruit ripening, the protein kinase FvMAPK6 acts downstream of FvMKK4 to phosphorylate FvRIF, thereby promoting its transcriptional activity. Activated FvRIF controls fruit ripening by regulating ripening-related genes directly or in an ABA-dependent pathway, which, in turn, modulates *FvRIF* expression by a positive feedback loop. FvRIF also functions by targeting numerous TF genes (i.e. *FvMYB10*, *FvSEP3*, *FvSPT*, and *FvARF2*), which regulate fruit ripening via control of ripening-related genes.

Discussion

RIF may act as an evolutionarily conserved regulator in controlling fruit ripening

As specific TFs in plants, NAC proteins participate in numerous physiological responses, including embryogenesis (Kunieda et al. 2008), leaf senescence (Liang et al. 2014), starch and protein accumulation (Zhang et al. 2019), and response to stresses (Shahnejat-Bushehri et al. 2016). In recent years, NAC TFs have been reported to play crucial roles in the ripening of climacteric and nonclimacteric fruits. In tomato, a typical climacteric fruit, the loss of function of SlNOR-like1, a member of the NAC TF family, dramatically inhibits fruit ripening (Gao et al. 2018). The fruits of plants carrying a mutation in this gene exhibit a significant reduction in ethylene production, a delay in softening and in the loss of chlorophyll, as well as reduced lycopene accumulation (Gao et al. 2018). The NAC proteins MaNAC1 and MaNAC2 from banana (*Musa acuminata*) (Shan et al. 2012) and PpBL in peach (*Prunus persica*) (Zhou et al. 2015), both of which are climacteric fruits, also play essential roles in fruit ripening. In watermelon (*Citrullus lanatus*), a nonclimacteric fruit, knockout of *ClNAC68*, the most highly expressed NAC TF gene, delays fruit development and decreases the soluble solid content and sucrose accumulation in fruit flesh (Wang et al. 2021). Moreover, CmNAC-NOR, a homolog of tomato SlNAC-NOR, functions as a key regulator of fruit ripening in melon, which has both climacteric and nonclimacteric fruit ripening varieties (Wang, Tian, et al. 2022). In the present study, we showed that FvRIF is essential for the ripening of strawberry, a typical nonclimacteric fruit. Mutation of *FvRIF* dramatically influences ripening (Fig. 1), consistent with the phenotypes previously observed in *FaRIF*-RNAi fruits (Martin-Pizarro et al. 2021). Considering that FvRIF exhibits 54.3% identity with SlNOR-like1 and 30.9% identity with ClNAC68 (Wang et al. 2021), we speculate that RIF, similar to MADS-RIN (RIPENING INHIBITOR) (Vrebalov et al. 2002; Vallarino et al. 2020), acts as a common regulator in controlling the ripening of both climacteric and nonclimacteric fruits. *RIF* holds the potential to serve as a target for molecular breeding to improve fruit quality or extend fruit shelf life. The function of genes homologous to *FvRIF* in other fruit species remains to be determined.

FvRIF directly regulates multiple aspects of ripening as a global regulator

The ripening of fleshy fruit is associated with dramatic changes in color, texture, flavor, and aroma (Giovannoni 2004). In our study, fruit firmness and contents of anthocyanin and sugar were substantially reduced in the *Fvrif* lines, suggesting that FvRIF functions as a global regulator controlling various ripening-related steps in strawberry fruit. To unravel the mechanisms underlying FvRIF-mediated transcriptional regulation in fruit ripening, we combined DAP-seq with RNA-seq, which uncovered 2,080 direct FvRIF-regulated target genes, including those involved in anthocyanin biosynthesis, cell-wall degradation, and sugar metabolism.

Anthocyanins constitute a group of naturally occurring pigments present in many flowers and fruits (Grotewold 2006). Besides their physiological roles in plants, such as attraction of pollinators and seed dispersers, anthocyanins are markers of ripening and contribute to the quality of fruits (Zhang et al. 2014). Anthocyanins are also recognized as compounds with health-promoting effects (Mattioli et al. 2020). The biosynthesis of anthocyanins is complicated and consists of a series of steps, although the structural genes responsible for anthocyanins biosynthesis are well defined. The regulation of anthocyanin biosynthesis is governed by TFs including R2R3 MYB TFs, MYC-like bHLH, and WD40-repeat proteins, which form a MYB–bHLH–WD40 regulatory complex (Schaart et al. 2013). In strawberry, MYB10 has been revealed as the primary activator of structural genes in the anthocyanin biosynthetic pathway during fruit ripening (Lin-Wang et al. 2010; Castillejo et al. 2020), but how MYB10 is transcriptionally activated by developmental regulators has not been defined. Furthermore, whether the structural genes in the anthocyanin biosynthetic pathway are regulated by other transcriptional regulators remains to be determined. In this study, we identified FvRIF as a ripening regulator that directly targets several structural genes in the anthocyanin biosynthetic pathway, i.e. *FvCHS1*, *FvDFR*, *FvANS*, and *FvUFGT*, and regulates their expression (Fig. 5, E and F). Intriguingly, we found that FvRIF binds to the promoter of *MYB10* and activates its transcription (Fig. 7). These data indicate that FvRIF can modulate anthocyanin biosynthesis directly by regulating the structural genes or indirectly by activating *MYB10* expression, encoding the specific regulator for anthocyanin biosynthesis. Our results uncover a regulatory network controlling anthocyanin biosynthesis during strawberry fruit ripening.

Fruit softening, a hallmark of ripening in most fleshy fruits is a major determinant of shelf life and commercial value (Wang et al. 2018). Softening of fleshy fruits is the consequence of multiple cellular decisions, including cell-wall disassembly and the depolymerization of cell-wall components (Wang et al. 2018). A complex set of cell-wall–degrading and cell-wall–modifying enzymes, such as PGs, PLs, pectin methylesterase (PME), and xyloglucan endotransglucosylase/hydrolases (XTHs), and a family of cell-wall proteins known as EXPs, are involved in the softening of fleshy fruits (Moya-Leon et al. 2019). Of these, PME and XTH display antagonistic effects on softening (Paniagua et al. 2014). In strawberry, the silencing of a *PL* gene (Jimenez-Bermudez et al. 2002), a *PG* (Quesada et al. 2009), or a gene encoding a TBG

(β-galactosidase) (Paniagua et al. 2016), using an antisense approach, reduced fruit softening. However, the regulation of these cell-wall–modifying enzymes in strawberry is still poorly understood. Recently, FaRIF was demonstrated to be associated with fruit softening in strawberry, and a number of cell-wall–modifying genes were downregulated in *FaRIF*-RNAi fruits (Martin-Pizarro et al. 2021), but the regulatory mechanisms remained unclear. In the present study, we provide several lines of evidence that FvRIF directly binds to the promoter of 4 genes encoding cell-wall–modifying enzymes and proteins (*FvPL2*, *FvPG2*, *FvXTH*, and *FvEXP3*) and regulates their expression, suggesting that FvRIF plays a direct role in the regulation of fruit softening in strawberry.

Besides genes associated with anthocyanin biosynthesis and cell-wall degradation, we also identified *FvPYR2*, encoding an ABA receptor, as a FvRIF-regulated direct target (Supplemental Data Set S8). ABA plays a critical role in controlling the ripening of nonclimacteric fruits, including strawberry (Chai et al. 2011; Li et al. 2011; Ji et al. 2012; Li, Grierson, et al. 2022). Several components in the ABA biosynthesis and signaling pathways, including the ABA biosynthesis rate-limiting enzyme NCED, the ABA receptors FaPYR and FaABAR (ABA-BINDING PROTEIN), the type 2C protein phosphatase FaABI1 (ABA-INSENSITIVE 1), and the SNF1-related kinase FaSnRK2.6, are indispensable for strawberry fruit ripening (Chai et al. 2011; Jia et al. 2011, 2013; Han et al. 2015; Liao et al. 2018). In a previous study, we demonstrated that the transcripts of *NCED5* and *ABAR* undergo m^6A-mediated posttranscriptional regulation, which enhances the mRNA stability of *NCED5* and promotes the translation efficiency of *ABAR* (Zhou et al. 2021), but modulation of these genes at the transcriptional level remains largely unknown. The identification of FvPYR2 as a direct target of FvRIF indicates that FvRIF contributes to the regulation of the ABA signaling pathway during strawberry fruit ripening. FvRIF may regulate ripening of strawberry fruit partially by targeting the ABA pathway. Considering that the expression of *FvRIF* is induced by ABA (Supplemental Fig. S11), we propose that ABA induces the expression of *FvRIF*, which in turn regulates the ABA pathway via a positive feedback loop to control strawberry fruit ripening. Notably, although *NCED5* and *SnRK2.6* exhibited differential expression in the *Fvrif* mutant lines (Supplemental Data Set S7), we did not identify them as FvRIF-bound genes in the DAP-seq analysis (Supplemental Data Set S4), suggesting that they appear to be indirectly regulated by FvRIF.

Intriguingly, our DAP-seq coupled with RNA-seq analysis suggested a total of 137 TF genes, which belong to multiple TF families (e.g. MYB, MADS-box, bHLH, and ARF), as direct targets of FvRIF. Besides *FvMYB10*, another 3 TF genes, *FvSEP3*, *FvSPT*, and *FvARF2*, have been previously characterized as regulators of strawberry fruit ripening. The direct regulation of these TFs by FvRIF (Fig. 7) suggests that FvRIF may control fruit ripening partly through modulating their expression. The roles of the remaining FvRIF target TF genes in strawberry fruit ripening remain unclear. Functional analysis of these TF genes will help to understand more comprehensively the ripening regulatory mechanism in strawberry.

pFvRIF modulates its activity

As an essential pathway for modification via protein phosphorylation, MAPK cascades are composed of a 3-kinase module: a MAPK kinase kinase (MAPKKK, also named MEKK and MKKK), a MAPK kinase (MAPKK, also named MEK and MKK), and a MAPK (MPK) (Stanko et al. 2014). Upon cellular stimulation, the MAPKKKs are activated, leading to phosphorylation and activation of a subset of downstream MAPKKs, which in turn activate the bottom tier MAPKs through phosphorylation (Stanko et al. 2014). The MAPK cascade is responsible for various biological events in *Arabidopsis*, including cell differentiation, development, stress responses, and phytohormone signaling (Nakagami et al. 2005). Compared to *Arabidopsis*, the regulatory effects of the MAPK pathway in horticultural crops have just begun to be explored.

In banana, the MaMPK6-3-mediated phosphorylation enhances the transcriptional activation function of bZIP21, a basic leucine zipper (bZIP) TF, on a subset of ripening-related genes, thereby stimulating fruit ripening (Wu et al. 2022). In apple (*Malus domestica*), the ethylene response factor MdERF17 is modulated by MdMPK4-mediated phosphorylation, which activates the transcriptional activity of MdERF17 and promotes fruit peel degreening during light/dark transitions (Wang, Wang, et al. 2022). Recently, it was reported in strawberry that a FvMKK4–FvMAPK3 module is responsible for the low-temperature–mediated repression of anthocyanin accumulation, partially through phosphorylating the TF FvMYB10 and reducing its transcriptional activity (Mao et al. 2022). This module implicates the MAPK pathway in the modulation of ripening in strawberry, although the regulatory networks remain largely unknown. In this study, we demonstrated that FvRIF interacts with FvMAPK6 and is phosphorylated by the FvMKK4–FvMAPK6 module at residue Thr-310, which positively regulates the transcriptional activation function of FvRIF (Figs. 8 to 10). Our results are in accordance with previous observation that NAC TFs are subject to MAPK-mediated phosphorylation, which exerts an effect on their activity (Liu et al. 2021; Xiang et al. 2021). Considering that FvMAPK6-mediated phosphorylation activates FvRIF, which in turn positively regulates FvMYB10, we speculate that FvMAPK6 plays a positive role in controlling *FvMYB10* expression. However, whether FvMAPK6 directly mediates phosphorylation of FvMYB10 and how it affects FvMYB10 activity remain unclear. Since FvMAPK3-mediated phosphorylation negatively regulates FvMYB10 (Mao et al. 2022), it seems likely that FvMAPK6 antagonizes FvMAPK3 in the regulation of FvMYB10, illustrating the complexity and rigorousness of MAPK-mediated regulation of their substrate proteins. The physiological role of FvMAPK6 and the interplay between FvMAPK3 and FvMAPK6 deserve further investigation.

In conclusion, this work unraveled the mechanisms underlying FvRIF-mediated transcriptional regulation of strawberry fruit ripening and identified the direct FvRIF-regulated target genes at the genome scale. Moreover, this study revealed the regulation of FvRIF activity by phosphorylation mediated by the FvMKK4–FvMAPK6 module. These findings provide insights into the regulatory network of FvRIF in controlling strawberry fruit ripening and highlight the crucial effect of protein phosphorylation on FvRIF activity during ripening.

Materials and methods

Plant materials and growth conditions

Diploid strawberry plants (*F. vesca*. cv Ruegen) were grown in the greenhouse at 22 °C under a 16-h light/8-h dark photoperiod under illumination provided by cool-white fluorescent light (with a light intensity of 200 to 300 μmol m^{-2} s^{-1}) with 70% relative humidity. Octoploid strawberry (*F.* × *ananassa* Duch. cv Benihoppe) were cultivated in a plastic greenhouse under standard culture conditions. Fruits of ''Ruegen' and 'Benihoppe' were harvested at the small green (SG), middle green (MG), large green (LG), turning fruit (TF), and red fruit (RF) stages mainly based on their size, shape, weight, and color. For 'Ruegen', the fruits at different stages corresponded approximately to 17, 20, 22, 25, and 26 DPA, respectively. All fruit samples were stripped of achenes and maintained at fresh status for analysis or directly frozen and stored at −80 °C.

Phylogenetic analysis

The amino acid sequence of FvRIF (FvH4_3g20700) in diploid woodland strawberry was acquired from the Genome Database for Rosaceae (GDR) database (https://www.rosaceae.org/species/fragaria/all). Other FvRIF homologous proteins from different species were obtained from the National Center for Biotechnology Information (NCBI) database (http://www.ncbi.nlm.nih.gov/). Multiple protein sequence alignments were carried out using DNAMAN software (version 8) with default parameters and are given in Supplemental File S1. The phylogenetic tree was reconstructed via the neighbor-joining method using MEGA software (version 10.1.8) with 500 bootstrap replicates (Thompson et al. 1997). The corresponding Newick tree is given in Supplemental File S2. The protein sequences of FvRIF and its homologous genes in other plants are provided in Supplemental File S3.

RNA isolation and RT-qPCR

Total RNA was isolated from 3 biological replicates of fruits using a FastPure Plant Total RNA Isolation Kit (Polysaccharides & Polyphenolics-rich) (Vazyme, China). Each biological replicate consisted of a pool of 3 to 5 fruits collected from 3 plants. Genomic DNA removal and cDNA synthesis were performed using HiScript II Q Select RT SuperMix for qPCR (+gDNA wiper) (Vazyme, China). qPCR was conducted using ChamQ SYBR qPCR Master Mix (Vazyme, China) on a StepOnePlus Real-Time PCR System (Applied Biosystems, USA) with the following program: 95 °C for 30 s, followed by 40 cycles of 95 °C for 10 s and 60 °C for 30 s. Relative quantitative gene expression values were calculated according to the cycle threshold (Ct) $2^{-\triangle\triangle Ct}$ method. Strawberry *ACTIN* (FvH4_6g22300) was used to normalize the expression values. The primers for RT-qPCR are listed in Supplemental Table S4.

CRISPR/Cas9 and overexpression vector construction and plant transformation

CRISPR/Cas9 vector construction was performed as described (Ma et al. 2015). Briefly, 2 specific sgRNAs targeting the coding region of *FvRIF* were designed using the website CRISPR-P 2.0 (http://crispr.hzau.edu.cn/CRISPR2/). Using a PCR-based method, the 2 sgRNAs were individually inserted into an expression cassette driven by the *AtU3b* or *AtU3d* promoter in a sgRNA intermediate plasmid. The 2 resulting expression cassettes were then incorporated into the pYLCRISPR/Cas9Pubi-H binary plasmid (Ma et al. 2015) using Golden Gate ligation. To construct the overexpression vector, the full-length coding sequence of *FvRIF* was amplified from cDNA of the diploid strawberry 'Ruegen' fruits and ligated into the pCAMBIA1302 plasmid under the CaMV 35S promoter to generate pCAMBIA1302-*HA-FvRIF* vector. The sgRNA sequences and primers used in vector construction are listed in Supplemental Table S5.

For the generation of transgenic strawberry plants, the above constructs were individually transformed into *Agrobacterium* (*Agrobacterium tumefaciens*) strain GV3101. *Agrobacterium* cultures were grown at 28 °C to a final OD_{600} of 0.5 and then used to infiltrate the diploid strawberry 'Ruegen' following a previously described method (Oosumi et al. 2006). Transgenic strawberry lines were selected based on hygromycin resistance (2 mg L^{-1}) and PCR screening. For CRISPR/Cas9-based knockouts, the transformants were screened at the targeted sites using PCR amplification and Sanger sequencing, and homozygous mutant lines in the second generation with desired editing were used for analyses. For transgenic overexpression plants, the presence and identity of the transgenes were confirmed by PCR genotyping. The primers used for screening the transgenic plants are listed in Supplemental Table S5.

Preparation of FvRIF-specific antibody

For FvRIF-specific antibody preparation, a fragment of *FvRIF* (*FvRIFt*) lacking the conserved domain was amplified from cDNA of the diploid strawberry 'Ruegen' fruits and cloned into the pET-30a vector (Merck KGaA, Germany). The resulting construct was produced in *Escherichia coli* Rosetta competent cells (TransGen Biotech, China) at 37 °C by induction with 1 mM isopropyl-1-thio-β-D-galactopyranoside (IPTG) for 5 h. Recombinant FvRIFt was isolated from *E. coli* and purified using Ni-NTA His Bind Resin (Merck KGaA, Germany) according to the manufacturer's manual. Following further purification by preparative gel electrophoresis, recombinant

FvRIFt was used to immunize rabbits by Abmart Co., Ltd (http://www.ab-mart.com.cn). The specific anti-FvRIF polyclonal antibody was affinity purified from rabbit antiserum using AminoLink Plus Coupling Resin according to the purification protocol (Thermo Scientific, USA). The primers used in vector construction are listed in Supplemental Table S5.

Extraction of nuclear proteins

Nuclei isolation was performed according to a previously described method (Wang et al. 2014). The nuclear proteins were obtained using phenol extraction as previously described (Saravanan and Rose 2004) with some modifications. In brief, the nuclei were fragmented by sonification on ice in 500 μL of extraction buffer (0.7 M sucrose, 0.1 M KCl, 0.5 M Tris-HCl pH 7.5, 0.5 M EDTA, 1 mM PMSF, and 5 mM β-mercaptoethanol), followed by mixing with an equal volume of Tris-HCl pH 7.5-saturated phenol for 10 min. After centrifugation at 16,000 × g for 10 min at 4 °C, the phenol phase was retained, washed, and precipitated by ice-cold saturated ammonium acetate in methanol. The precipitated proteins were collected by centrifugation at 12,000 × g for 5 min at 4 °C and washed with ice-cold methanol followed by multiple ice-cold acetone washes. Proteins were air-dried and stored at −80 °C until use.

Immunoblot analysis

Immunoblot analysis was performed as previously described (Wang et al. 2014). Proteins were separated by 10% (w/v) SDS–PAGE and then electro-transferred onto an Immobilon-P PVDF membrane (Millipore, USA) using a semi-dry transblotter Trans-Blot Turbo (Bio-Rad, USA). Following incubation with blocking buffer (5% [w/v] skim milk in TBS containing 0.05% [v/v] TBST) for 1 h, the PVDF membrane was incubated with specific antibody for 1 h. After washing 4 times with TBST, the PVDF membrane was incubated with horseradish peroxidase (HRP)-conjugated anti-rabbit IgG secondary antibody. The immunoreactive bands were visualized with a chemiluminescence detection kit (Mei5 Biotechnology Co., Ltd, China) according to the manufacturer's protocol.

Anthocyanin measurement

Anthocyanins were extracted and measured as previously described (Cheng et al. 2014) with minor modifications. In brief, fruits were finely ground to powder with liquid nitrogen, and approximately 0.5 g of fruit powder was weighed out into 1 mL of 1% (v/v) HCl–methanol solution. Following ultrasonic extraction at 600 W for 30 min at 30 °C in the dark, the homogenates were centrifuged at 12,000 × g for 10 min at 4 °C and then filtered through 0.22-μm Millipore membranes (Millipore, USA). The resulting supernatants were subjected to HPLC analysis on an ACQUITY UPLC system (Waters, USA) equipped with a C18 column according to the manufacturer's recommendations. The experiment was performed with 3 biological replicates. For each replicate, 5 fruits from 3 plants were pooled to account for variation among individuals. Cyanidin-3-glucoside (C3G) was used as standard.

Measurement of fruit firmness

Fruit firmness was tested at the equator of fruits using the puncture method with a 2-mm diameter probe on a texture analyzer (Food Technology Corporation, USA). Three biological replicates were performed, and each replicate contained at least 3 fruits from each sample.

Determination of soluble sugar content

For soluble sugar analysis, strawberry fruit powder (1 g) was mixed with 5 mL of double distilled water and incubated in a water bath for 30 min at 100 °C. After centrifugation at 10,000 × g for 10 min at 25 °C, the supernatant was collected. HPLC analysis was then performed on an LC-10ATVP HPLC system (Shimadzu, Japan), with a refractive index detector RID-10A (Shimadzu, Japan). Separation was performed on a Dikma Polyamino HILIC column (5 μm, 250 mm × 4.6 mm) with a column temperature of 30 °C and an injection volume of 10 μL at a flow rate of 1 mL min^{-1}. D-(+) glucose, D-(−) fructose, and sucrose (Sigma-Aldrich, USA) were used as standards. The entire procedure was performed 3 times. For each replicate, 5 fruits from 3 plants were pooled to account for variation among individuals.

DAP-seq and data analysis

DAP-seq was carried out according to the procedure previously described (O'Malley et al. 2016; Bartlett et al. 2017). In brief, a 'Ruegen' genomic DNA library was prepared using a NEBNextDNA Library Prep Master Mix Set Kit for Illumina (NEB, USA). Recombinant FvRIF was produced as a fusion protein with the HaloTag sequence (Promega, USA) using a TNT SP6 High-Yield Wheat Germ Protein Expression System (Promega, USA). Recombinant FvRIF-HaloTag was purified with HaloTag Beads (Promega, USA), and the FvRIF-HaloTag beads mixtures or HaloTag beads (input negative control) were directly used to incubate with the 'Ruegen' genomic DNA library in the incubation buffer (1 × phosphate-buffered saline [PBS], 0.005% [v/v] IGEPAL CA-630) under slow rotation at 4 °C for 2 h. After washing 5 times with PBS, the DNA fragments were eluted from the FvRIF-HaloTag beads with elution buffer (50 mM Tris-HCl, pH 8.5). DAP-seq library was constructed using a KAPA Library Quantification Kit (KAPA, USA) and then subjected to high-throughput sequencing analysis on a Nova S4 instrument as 150-b paired-end reads (Illumina, USA).

For DAP-seq data analysis, clean DAP-seq reads were mapped to the *F. vesca* reference genome with the 4.0 a1 annotation (https://www.rosaceae.org/species/fragaria_vesca/genome_v4.0.a1). DAP-seq peaks were identified by MACS2 (version 2.1.1) (Zhang et al. 2008) using default parameters ($q < 0.05$). Only peaks present in both biological replicates were selected as confident peaks for analysis. The FvRIF binding regions included promoter (up to 2-kb upstream from the TSS), intergenic region, intron, exon, 3′ UTR, and 5′

UTR. The gene closest to the FvRIF binding sites were defined as FvRIF-binding gene when searched with PeakAnnotator (Kondili et al. 2017). The enriched peaks were visualized with Integrative Genomics Viewer (IGV, version 2.8.2) (Robinson et al. 2011). Motifs were discovered using Homer version 3 (Heinz et al. 2010). GO enrichment analysis was performed based on the Gene Ontology Resource database (http://geneontology.org/).

RNA-seq and data analysis

Total RNA was isolated from 3 biological replicates of fruits from wild type and the mutant lines. Each replicate consisted of a pool of 10 fruits collected from 3 plants. The cDNA libraries were prepared and sequenced on an Illumina sequencing platform (Illumina novaseq 6000). Raw RNA-seq reads were filtered using fastp (Chen et al. 2018) and then mapped to the *F. vesca* reference genome 4.0 a1 (https://www.rosaceae.org/species/fragaria_vesca/genome_v4.0.a1) using HISAT2 (Kim et al. 2015). Gene expression was expressed as fragments per kilobase of exon per million mapped fragments (FPKM) with featureCounts (Liao et al. 2014). DEGs were analyzed using DESeq2 v1.22.1 (Love et al. 2014) with the *P*-value being corrected by the Benjamini–Hochberg method. Genes with a FDR < 0.05 and $\text{Log}_2(\text{FC}) > 1$ or $\text{Log}_2(\text{FC}) < -1$ were considered as DEGs. For KEGG enrichment, a hypergeometric distribution test was performed with the unit of the pathway using KEGG Compound database (https://www.genome.jp/kegg/compound/). GO enrichment analysis was performed based on the Gene Ontology Resource database (http://geneontology.org/). All enrichment data were visualized with ImageGP software (http://www.ehbio.com/ImageGP).

Yeast hybrid assays (Y1H and Y2H)

The Y1H assay was performed according to the Matchmaker Gold Yeast One-Hybrid Library Screening System user manual (Clontech, USA). The coding sequence of *FvRIF* was amplified from cDNA of the diploid strawberry 'Ruegen' fruits and ligated into the pGADT7 vector (Clontech, USA) to generate pGADT7-*FvRIF*. The specific DNA sequences (200 bp) from promoters of the target genes were amplified from genomic DNA of 'Ruegen' fruits and individually cloned into the pAbAi vector (Clontech, USA). The resulting pAbAi vectors, which contain the target gene sequences, were transformed into the yeast (*S. cerevisiae*) strain Y1H Gold and spread onto synthetic defined (SD)/−Ura medium (Clontech, USA). Positive colonies were spread onto agar-solidified dextrose SD/−Ura medium with various concentrations of AbA to screen for an appropriate concentration and eliminate self-activation. The pGADT7-*FvRIF* was then transformed into the positive colonies and spread onto SD/−Leu medium containing an appropriate AbA concentration. pAbAi-*pro53* and empty pGADT7 were used as positive and negative controls, respectively. The primers used in vector construction are listed in Supplemental Table S5.

The Y2H assay was carried out based with the GAL4-based Two-Hybrid System according to the manufacturer's instructions (Clontech, USA). The coding sequence of *FvMAPK6* was cloned into pGBKT7 to generate pGBKT7-*FvMAPK6*. The resulting pGBKT7-*FvMAPK6* and pGADT7-*FvRIF* constructs were cotransformed into yeast strain AH109 and grown on minimal SD medium lacking Leu and Trp (−LW) or lacking Leu, Trp, His, and Ade (−LWHA). The transformants carrying empty vectors (BD or AD) were used as negative controls. The primers used for vector construction are listed in Supplemental Table S5.

EMSA

The full-length *FvRIF* coding sequence was cloned into pCold-TF-His vector (Takara, Japan) and then transformed into *E. coli* BL21 (DE3). To obtain soluble His-FvRIF proteins, *E. coli* containing pCold-TF-His-*FvRIF* was cultured at 16 °C for 24 h with induction of 1 mM IPTG. Recombinant His-FvRIF was isolated from *E. coli* and purified using Ni-NTA His Bind Resin (Merck KGaA, USA) following the manufacturer's manual. The 5′ biotin-labeled double-stranded DNA probes were prepared by annealing 5′ biotin-labeled oligonucleotides to the corresponding complementary strands. EMSA was performed using a Lightshift Chemiluminescent EMSA kit (Thermo Scientific, USA) according to the standard protocol with some modifications. In brief, recombinant His-FvRIF was incubated with labeled or nonlabeled double-stranded probes at room temperature for 20 min. The samples were separated by 6% (w/v) native polyacrylamide gels at 4 °C in the dark for 1 h, and then the biotin-labeled probes was captured using a Tanon imaging system (Tanon, China). The oligonucleotide probes used in this study are listed in Supplemental Table S6.

ChIP

The ChIP assay was performed as described previously (Wang et al. 2014) with minor modifications. The fruits (with achenes stripped) at 24 DPA from wild type and the *Fvrif-13-* mutant line were sliced and fixed in 1% (w/v) formaldehyde under vacuum for 10 min. The cross-linked fruits were subjected to nuclear isolation as described above, and the enriched nuclei were then treated by sonication at 30% power for 2 min on ice (SONICS Vibra-Cell VCX150, USA) to shear the chromatin to an average size of 250 to 1,500 bp. A small aliquot of the sonicated chromatin was reverse cross-linked and used as the input DNA control.

The remaining sheared chromatin was incubated with affinity-purified polyclonal anti-FvRIF antibody that was coated overnight at 4 °C on the Magna ChIP Protein A + G Magnetic Beads (Millipore, USA) as previously described (Wang et al. 2014). After incubation for 4 h at 4 °C, the beads were collected by magnetic rack and washed sequentially for 10 min at 4 °C with low-salt buffer (150 mM NaCl, 0.1% SDS, 1% Triton X-100, 2 mM EDTA, and 20 mM Tris-HCl pH 8.0), high-salt buffer (500 mM NaCl, 0.1% SDS, 1% Triton X-100, 2 mM EDTA, and 20 mM Tris-HCl pH 8.0), lithium chloride

buffer (0.25 M LiCl, 0.5% NP-40, 1 mM EDTA, 10 mM Tris-HCl pH 8.0, and 0.5% sodium deoxycholate), and TE buffer (10 mM Tris-HCl pH 8.0, and 1 mM EDTA). The DNA–protein complexes were eluted from the beads by occasional rotation at 65 °C for 1 h. The cross-linking between immunoprecipitated DNA and FvRIF protein was reversed by adding NaCl to a final concentration of 0.2 M, and the eluate was incubated overnight at 65 °C. After recovery of the immunocomplexes by reverse cross-linking, the immunoprecipitated DNA was further purified using a TIANquick Mini Purification Kit (TIANGEN, China). The primers used for quantitative PCR were designed based on the FvRIF binding motifs identified by DAP-seq and are listed in Supplemental Table S3. Each ChIP assay was carried out 3 times, and the enriched DNA fragments in each ChIP sample served as 1 biological replicate for qPCR.

LCI assay

The LCI assay was carried out as previously described (Chen et al. 2008). The coding sequences of *FvMAPK6* and *FvRIF* were individually amplified from cDNA of the diploid strawberry 'Ruegen' fruits and separately ligated into the pCAMBIA1300-cLUC/nLUC vectors (provided by Prof. Jianmin Zhou from the Institute of Genetics and Developmental Biology, Chinese Academy of Sciences), which were then individually introduced into *Agrobacterium* strain GV3101. After incubation at 28 °C for 24 h, the *Agrobacteria* containing the recombinant cLUC constructs were mixed with an equal volume of *Agrobacteria* containing recombinant nLUC constructs and then infiltrated into *N. benthamiana* leaves. After being grown for 48 h, the leaves were sprayed with 1 mM D-luciferin dissolved in ddH_2O containing 0.01% (v/v) Triton X-100 and then kept in the dark for 5 min. Luminescence images were captured using a chemiluminescence imaging system (Tanon, China). The *N. benthamiana* leaves infiltrated with empty vectors expressing *cLUC* or *nLUC* were used as negative controls. The experiment was performed with at least 3 *N. benthamiana* leaves. The primers used for the generation of LCI constructs are listed in Supplemental Table S5.

Pull-down assay

To produce the MBP-FvRIF and GST-FvMAPK6 recombinant proteins, the coding sequence of *FvRIF* was amplified and cloned into the pMAL-c2X-MBP vector (NEB, USA) and the coding sequence of *FvMAPK6* was inserted into the pGEX-6P-1-GST (GE Healthcare, USA), respectively. The resulting constructs were introduced into *E. coli* Rosetta competent cells (TransGen Biotech, China). To obtain soluble recombinant MBP-FvRIF and GST-FvMAPK6, *E. coli* colonies were cultured at 16 °C for 24 h with induction of 1 mM IPTG. The purification of MBP-FvRIF was conducted as described previously (Wang et al. 2020), while the purification of GST-FvMAPK6 was performed using glutathione Sepharose beads (GE Healthcare, USA) according to the manufacturer's manual. For pull-down assays, GST or GST-FvMAPK6 bound to glutathione Sepharose beads was directly incubated with MBP-FvRIF at 4 °C for 2 h in NETN buffer (20 mM Tris-HCl, 100 mM NaCl, 0.5 mM EDTA, and 0.5% [v/v] IGEPAL CA-630, pH 8.0). After washing 3 times with elution buffer (50 mM Tris-HCl, 0.1% [v/v] NP-40, and 200 mM NaCl), the proteins bound to beads were eluted and subjected to immunoblotting analysis with anti-GST antibody (1:5,000 dilutions; Abmart, China) and anti-MBP antibody (1:5,000 dilutions; Abmart, China), respectively. The primers used for vector construction are listed in Supplemental Table S5.

Co-IP analysis

The Co-IP assay was carried out as previously described (Wang et al. 2020). The coding sequence of *FvMAPK6* amplified from cDNA of the diploid strawberry 'Ruegen' fruits was cloned into the pCAMBIA1300-Flag-MCS vector. The resulting pCAMBIA1300-*FvMAPK6-Flag* and the pCAMBIA1302-*HA-FvRIF* generated as described above were then individually introduced into *Agrobacterium* strain GV3101. The empty vector was used as a negative control. The *Agrobacterium* strains each containing *FvMAPK6-Flag* or *HA-FvRIF* were coinfiltrated into *N. benthamiana* leaves. After incubation at 25 °C for 48 h, total proteins were extracted from the leaves with 1 mL of extraction buffer (50 mM Tris-HCl, pH 7.5, 100 mM NaCl, 1 mM EDTA, 1% [v/v] Triton X-100, 5% [v/v] glycerol, 1 mM PMSF, and 1 × protease inhibitor cocktail) and then immunoprecipitated with anti-HA magnetic beads (LABLEAD, China) or anti-Flag magnetic beads (MBL Life Science, Japan) at 4 °C for 2 h. The beads were collected and washed 3 times with extraction buffer. The proteins were eluted from the beads with 1 × SDS loading buffer at 95 °C for 5 min and then subjected to immunoblotting using anti-HA (Abcam, UK) or anti-Flag (MBL Life Science, Japan) antibodies, respectively. The primers used for generation of constructs are listed in Supplemental Table S5.

Subcellular localization

For localization analysis, the coding sequences of *FvMAPK6* and *FvRIF* were amplified from cDNA of the diploid strawberry 'Ruegen' fruits and inserted into the pCAMBIA2300-mCherry and pCAMBIA2300-eGFP vector to produce *35S:FvMAPK6-mCherry* and *35S:FvRIF-eGFP*, respectively. The resulting plasmids were separately transformed into *Agrobacterium* strain GV3101, which was subsequently infiltrated or coinfiltrated into *N. benthamiana* leaves (Sparkes et al. 2006). The *N. benthamiana* plants were cultured in the greenhouse for 48 h, and then mesophyll protoplasts were isolated (Lei et al. 2015). GFP and mCherry fluorescence signals were observed and captured by confocal microscopy (Zeiss, Germany). H2B-mCherry served as a nuclear marker. The primers used for vector construction are listed in Supplemental Table S5.

Phosphorylation assay and phosphorylation site identification

In vitro phosphorylation assays were performed as previously described (Li, Liu, et al. 2022). The coding sequence of *FvRIF*

was cloned into pCold-TF-His vector (Takara, Japan) and transformed into *E. coli* BL21 (DE3) to generate recombinant His-FvRIF-HA. To produce recombinant His-FvMKK4^{DD}, the T227D/S233D (DD) point mutations were introduced into *FvMKK4* (*FvMKK4*^{DD}), which was cloned into the pCold-TF-His vector (Takara, Japan) and produced in *E. coli* BL21 (DE3). For phosphorylation assays, recombinant GST-FvMAPK6 as described above was incubated with His-FvMKK4^{DD} in a kinase reaction buffer (25 mM Tris-HCl, pH 7.5, 10 mM $MgCl_2$, 1 mM DTT, and 50 μM ATP) at 25 °C for 30 min. Then, recombinant His-FvRIF-HA or the mutated variants (FvRIF^{S271A}, FvRIF^{S283A}, FvRIF^{S294A}, FvRIF^{S299A}, FvRIF^{T310A}, and FvRIF^{5A}) generated by site-directed mutagenesis were incubated with activated FvMAPK6 in kinase reaction buffer at 25 °C for 30 min. For alkaline phosphatase treatment, 0, 150, or 500 U of fast alkaline phosphatase (Thermo Fisher, USA) were added to the above kinase reaction buffer, followed by gentle mixing and incubation at 30 °C for 30 min. The reaction was terminated by the addition of 1 × SDS loading buffer, and the reaction products were then separated by 6% (w/v) SDS–PAGE gel containing 60 μM Phos-tag acrylamide (Wako, Japan) and 120 μM $MnCl_2$. The immunoblotting analysis was conducted as described above using anti-HA antibody (Abcam, UK). The gels without Phos-tag and $MnCl_2$ were stained with Coomassie brilliant blue (CBB) to indicate uniform sample loading. The primers used for vector construction are listed in Supplemental Table S5.

For LC-MS/MS assay, samples were prepared as for the in vitro phosphorylation assay. The samples were reduced, alkylated, and digested with trypsin (Promega, USA) and chymotrypsin (Promega, USA), respectively, followed by LC-MS/MS analysis. Samples were dissolved in solvent A (0.1% [v/v] formic acid in water) and then injected into a manually packed reverse phase C18 column (25-cm length, 150-μm inner diameter; C18 resin with 1.9-μm particle size; 120-Å pore diameter; Dr. Maisch GmbH Inc., Germany), which was connected to an Easy nLC-1200 nanoLC system (Thermo Fisher Scientific, Waltham, MA). The samples were eluted using a 70-min gradient at a flow rate of 600 nL/min (8% to 28% solvent B [0.1% formic acid and 20% water in acetonitrile] for 45 min, 28% to 40% solvent B for 15 min, 40% to 90% solvent B for 1 min and 90% solvent B for 9 min; all v/v). A Thermo Orbitrap Fusion Lumos mass spectrometer (Thermo Fisher Scientific, USA) was used for sample analysis using Thermo Scientific Xcalibur software (4.3) with the following parameters: the resolution was set to 120 K for MS1. In MS1, the scan range was 350 to 1,550 m/z. The automatic gain control was 4×10^5 and the charge state was 2 to 7. In MS2, the normalized collision energy was set to 32%. Ions were broken by higher collision dissociation and were then analyzed by Orbitrap with AGC targets set at 5×10^4.

Phosphorylation site identification was performed with Proteome Discoverer (v2.4) software, and the SEQUEST search engine was used. For the analysis of proteomic data, precursor mass tolerance was set to 20 ppm with a fragment mass tolerance of 0.05 Dalton. The enzyme used was trypsin/p, and the maximum missed cleavage was set to 2. Carbamidomethyl (C) was set as fixed modification with variable modifications of phosphorylation (STY), oxidation (M), and acetyl (Protein N-term) for all software programs. The rest of the parameters were set to default. *F. vesca* v4.0.a1.fasta.gz was downloaded from the GDR website (https://www.rosaceae.org).

GUS activity assay

GUS activity assay was performed as previously described (Mao et al. 2022). The full-length coding sequences of *FvRIF*, *FvRIF*^{T310A}, *FvMAPK6*, and *FvMKK4*^{DD} were individually inserted into pCAMBIA1301 vector under the control of the 35S promoter. The *FvCHS1* promoter (2,000-bp upstream of the ATG) from genomic DNA was ligated into the pCAMBIA1301 vector for driving the *GUS* reporter gene. The resulting constructs were individually transformed into *Agrobacterium* strain GV3101. The *Agrobacterium* cultures were resuspended in infiltration buffer (10 mM MES pH 5.6, 10 mM $MgCl_2$, and 200 mM acetosyringone) to a final OD_{600} of 0.6 for each construct and then injected into octoploid strawberry fruits at the LG stage according to the method previously described (Wei et al. 2018). After 4 d of incubation at 25 °C, the agroinfiltrated fruits were collected and frozen in liquid nitrogen. GUS activity was detected as described (Wei et al. 2018). The experiment was performed with 3 independent biological replicates, each consisting of 15 fruits. The primers used for vector construction are listed in Supplemental Table S5.

Transient gene expression in strawberry fruit

The transient gene expression in fruits of the *Fvrif* mutant lines was carried out following the method described previously (Gao et al. 2020). In brief, the coding sequences of *FvRIF* and *FvRIF*^{T310A} were ligated into the pCAMBIA1302 plasmid under the 35S promoter to generate *35S:FvRIF-HA* and *35S:FvRIF*^{T310A}*-HA* constructs. The *FvRIF* promoter (2,000-bp upstream of ATG) and the coding region from genomic DNA was cloned into the pCAMBIA1302 vector to generate the *FvRIFpro:FvRIF-HA* construct. The resulting constructs were separately transformed into *Agrobacterium* strain GV3101, which were subsequently injected into the fruits of the *Fvrif-13* mutant at the LG stage. The empty vector served as the negative control. More than 10 fruits were injected for each construct. The injected fruits were left on the plants to continue growth and fruit coloration appeared about 1 wk after injection.

Accession numbers

Sequence data from this article can be found in Supplemental File S4.

DAP-seq data sets were deposited at the Gene Expression Omnibus at NCBI under the accession number GSE220785. RNA-seq data sets were deposited at the Gene

Expression Omnibus at NCBI under the accession number GSE220768.

Acknowledgments

We would like to thank Zhuang Lu (Institute of Botany, Chinese Academy of Sciences) for analysis of MS/MS and Jingquan Li (Institute of Botany, Chinese Academy of Sciences) for assistance with confocal microscopy. We thank Yaoguang Liu (South China Agriculture University) for providing the pYLCRISPR/Cas9Pubi-H binary vector. We also thank Wuhan IGENEBOOK Biotechnology Co., Ltd for DAP-seq data analysis.

Author contributions

G.Q., D.P., and X.L. conceived and designed the research. X.L., C.M.-P., L.Z., B.H., and Y.W. performed the experiments. Y.S., B.L., and D.P. provided discussions. G.Q. and X.L. analyzed the data and wrote the article.

Supplemental data

The following materials are available in the online version of this article.

Supplemental Figure S1. Protein sequence alignment of FvRIF and FaRIF from diploid strawberry and octoploid strawberry.

Supplemental Figure S2. Expression pattern of *FaRIF* homologous genes in diploid strawberry.

Supplemental Figure S3. Full immunoblot for Fig. 1F.

Supplemental Figure S4. Off-target analysis in *Fvrif-6* and *Fvrif-13* mutants.

Supplemental Figure S5. Phenotypes of strawberry mutated for or overexpressing *FvRIF*.

Supplemental Figure S6. Phenotypes of the *Fvrif-1* mutant line.

Supplemental Figure S7. Analysis of the FvRIF binding site width and genome-wide overview of binding peaks.

Supplemental Figure S8. A high Pearson's correlation coefficient indicates a high similarity between the 2 *Fvrif* mutant lines.

Supplemental Figure S9. *FvRIF* expression levels in genome-edited diploid strawberry.

Supplemental Figure S10. Expression levels of well-known ripening-related genes in genome-edited diploid strawberry.

Supplemental Figure S11. ABA induces the expression of *FvRIF* in strawberry fruits.

Supplemental Figure S12. Genomic DNA and affinity-purified anti-FvRIF polyclonal antibody used for ChIP assay.

Supplemental Figure S13. Identification of FvRIF sites phosphorylated by FvMAPK6 via LC-MS/MS.

Supplemental Table S1. Number of total clean sequencing reads and mapping rate for each replicate of DAP-seq.

Supplemental Table S2. *F. vesca* ID numbers of genes mentioned in this work.

Supplemental Table S3. List of primers used for ChIP-qPCR analysis.

Supplemental Table S4. List of primers used for RT-qPCR analysis.

Supplemental Table S5. List of primers used in vector construction.

Supplemental Table S6. Sequences of the probes used in EMSA.

Supplemental Data Set S1. List of DAP-seq enriched peaks in Biological Replicate 1.

Supplemental Data Set S2. List of DAP-seq enriched peaks in Biological Replicate 2.

Supplemental Data Set S3. List of DAP-seq enriched peaks in both biological replicates.

Supplemental Data Set S4. List of FvRIF binding peaks within promoter regions in both biological replicates.

Supplemental Data Set S5. List of DEGs in *Fvrif-6* line by RNA-seq.

Supplemental Data Set S6. List of DEGs in *Fvrif-13* line by RNA-seq.

Supplemental Data Set S7. List of DEGs both in *Fvrif-6* and *Fvrif-13* lines by RNA-seq.

Supplemental Data Set S8. List of FvRIF-regulated direct target genes.

Supplemental Data Set S9. List of FvRIF-regulated direct target genes encoding TFs.

Supplemental Data Set S10. Summary of statistical analyses.

Supplemental File S1. Multiple sequence alignments used to generate the phylogenetic tree shown in Fig. 1A.

Supplemental File S2. Newick format of the phylogenetic tree shown in Fig. 1A.

Supplemental File S3. Full-length protein sequences for the phylogenetic tree shown in Fig. 1A.

Supplemental File S4. Full-length coding sequences and protein sequences for FvRIF, FvMAPK6, and FvMKK4.

Funding

This work was supported by the National Natural Science Foundation of China (31925035 to G.Q. and 32030100 to Y.S.), the Shandong Provincial Key Research and Development Program (2022TZXD0023 to G.Q.), the European Research Council (ERC-2014-Stg 638134 to D.P.), the Spanish Ministry of Science and Innovation (PID2021-123677OB-I00 to D.P.), and the Junta de Andalucía (UMA20-FEDERJA-093 and POSTDOC21_00893 to C.M.-P.).

Conflict of interest statement. The authors declare that there is no conflict of interest.

References

Aharoni A, De Vos CH, Wein M, Sun Z, Greco R, Kroon A, Mol JN, O'Connell AP. The strawberry FaMYB1 transcription factor suppresses anthocyanin and flavonol accumulation in transgenic tobacco. Plant J. 2001:**28**(3):319–332. https://doi.org/10.1046/j.1365-313X.2001.01154.x

Bartlett A, O'Malley RC, Huang S-s, Galli M, Nery JR, Gallavotti A, Ecker JR. Mapping genome-wide transcription-factor binding sites using DAP-seq. Nat Protoc. 2017:**12**(8):1659–1672. https://doi.org/10.1038/nprot.2017.055

Basu A, Nguyen A, Betts NM, Lyons TJ. Strawberry as a functional food: an evidence-based review. Crit Rev Food Sci Nutr. 2014:**54**(6):790–806. https://doi.org/10.1080/10408398.2011.608174

Castillejo C, Waurich V, Wagner H, Ramos R, Oiza N, Munoz P, Trivino JC, Caruana J, Liu Z, Cobo N, et al. Allelic variation of MYB10 is the major force controlling natural variation in skin and flesh color in strawberry (*Fragaria spp*.) fruit. Plant Cell 2020:**32**(12):3723–3749. https://doi.org/10.1105/tpc.20.00474

Chai L, Shen Y-Y. FaABI4 is involved in strawberry fruit ripening. Sci Hortic. 2016:**210**(10):34–40. https://doi.org/10.1016/j.scienta.2016.07.015

Chai YM, Jia HF, Li CL, Dong QH, Shen YY. FaPYR1 is involved in strawberry fruit ripening. J Exp Bot. 2011:**62**(14):5079–5089. https://doi.org/10.1093/jxb/err207

Chen HM, Zou Y, Shang YL, Lin HQ, Wang YJ, Cai R, Tang XY, Zhou JM. Firefly luciferase complementation imaging assay for protein-protein interactions in plants. Plant Physiol. 2008:**146**(2):368–376. https://doi.org/10.1104/pp.107.111740

Chen S, Zhou Y, Chen Y, Gu J. fastp: an ultra-fast all-in-one FASTQ preprocessor. Bioinformatics 2018:**34**(17):i884–i890. https://doi.org/10.1093/bioinformatics/bty560

Cheng J, Niu Q, Zhang B, Chen K, Yang R, Zhu JK, Zhang Y, Lang Z. Downregulation of RdDM during strawberry fruit ripening. Genome Biol. 2018:**19**(1):212. https://doi.org/10.1186/s13059-018-1587-x

Cheng J, Wei G, Zhou H, Gu C, Vimolmangkang S, Liao L, Han Y. Unraveling the mechanism underlying the glycosylation and methylation of anthocyanins in peach. Plant Physiol. 2014:**166**(2):1044–1058. https://doi.org/10.1104/pp.114.246876

Daminato M, Guzzo F, Casadoro G. A SHATTERPROOF-like gene controls ripening in non-climacteric strawberries, and auxin and abscisic acid antagonistically affect its expression. J Exp Bot. 2013:**64**(12):3775–3786. https://doi.org/10.1093/jxb/ert214

Edger PP, Poorten T, VanBuren R, Hardigan MA, Colle M, McKain MR, Smith RD, Teresi S, Nelson ADL, Wai CM, et al. Origin and evolution of the octoploid strawberry genome. Nat Genet. 2019:**51**(3):541–547. https://doi.org/10.1038/s41588-019-0356-4

Ernst HA, Olsen AN, Larsen S, Lo Leggio L. Structure of the conserved domain of ANAC, a member of the NAC family of transcription factors. EMBO Rep. 2004:**5**(3):297–303. https://doi.org/10.1038/sj.embor.7400093

Fenn MA, Giovannoni JJ. Phytohormones in fruit development and maturation. Plant J. 2021:**105**(2):446–458. https://doi.org/10.1111/tpj.15112

Filtz TM, Vogel WK, Leid M. Regulation of transcription factor activity by interconnected post-translational modifications. Trends Pharmacol Sci. 2014:**35**(2):76–85. https://doi.org/10.1016/j.tips.2013.11.005

Galli M, Khakhar A, Lu Z, Chen Z, Sen S, Joshi T, Nemhauser JL, Schmitz RJ, Gallavotti A. The DNA binding landscape of the maize AUXIN RESPONSE FACTOR family. Nat Commun. 2018:**9**(1):4526. https://doi.org/10.1038/s41467-018-06977-6

Gao Q, Luo H, Li Y, Liu Z, Kang C. Genetic modulation of *RAP* alters fruit coloration in both wild and cultivated strawberry. Plant Biotechnol J. 2020:**18**(7):1550–1561. https://doi.org/10.1111/pbi.13317

Gao Y, Wei W, Zhao XD, Tan XL, Fan ZQ, Zhang YP, Jing Y, Meng LH, Zhu BZ, Zhu HL, et al. A NAC transcription factor, NOR-like1, is a new positive regulator of tomato fruit ripening. Hortic Res. 2018:**5**(12):75. https://doi.org/10.1038/s41438-018-0111-5

Giampieri F, Alvarez-Suarez JM, Battino M. Strawberry and human health: effects beyond antioxidant activity. J Agric Food Chem. 2014:**62**(18):3867–3876. https://doi.org/10.1021/jf405455n

Giovannoni JJ. Genetic regulation of fruit development and ripening. Plant Cell 2004:**16**(suppl_1):S170–S180. https://doi.org/10.1105/tpc.019158

Grotewold E. The genetics and biochemistry of floral pigments. Annu Rev Plant Biol. 2006:**57**(1):761–780. https://doi.org/10.1146/annurev.arplant.57.032905.105248

Han Y, Dang R, Li J, Jiang J, Zhang N, Jia M, Wei L, Li Z, Li B, Jia W. SUCROSE NONFERMENTING1-RELATED PROTEIN KINASE2.6, an ortholog of OPEN STOMATA1, is a negative regulator of strawberry fruit development and ripening. Plant Physiol. 2015:**167**(3):915–930. https://doi.org/10.1104/pp.114.251314

Heinz S, Benner C, Spann N, Bertolino E, Lin YC, Laslo P, Cheng JX, Murre C, Singh H, Glass CK. Simple combinations of lineage-determining transcription factors prime *cis*-regulatory elements required for macrophage and B cell identities. Mol Cell. 2010:**38**(4):576–589. https://doi.org/10.1016/j.molcel.2010.05.004

Hoffmann T, Kalinowski G, Schwab W. RNAi-induced silencing of gene expression in strawberry fruit (*Fragaria* × *ananassa*) by agroinfiltration: a rapid assay for gene function analysis. Plant J. 2006:**48**(5):818–826. https://doi.org/10.1111/j.1365-313X.2006.02913.x

Ji K, Chen P, Sun L, Wang Y, Dai S, Li Q, Li P, Sun Y, Wu Y, Duan C, et al. Non-climacteric ripening in strawberry fruit is linked to ABA, FaNCED2 and FaCYP707A1. Funct Plant Biol. 2012:**39**(4):351–357. https://doi.org/10.1071/FP11293

Jia HF, Chai YM, Li CL, Lu D, Luo JJ, Qin L, Shen YY. Abscisic acid plays an important role in the regulation of strawberry fruit ripening. Plant Physiol. 2011:**157**(1):188–199. https://doi.org/10.1104/pp.111.177311

Jia HF, Lu D, Sun JH, Li CL, Xing Y, Qin L, Shen YY. Type 2C protein phosphatase ABI1 is a negative regulator of strawberry fruit ripening. J Exp Bot. 2013:**64**(6):1677–1687. https://doi.org/10.1093/jxb/ert028

Jimenez-Bermudez S, Redondo-Nevado J, Munoz-Blanco J, Caballero JL, Lopez-Aranda JM, Valpuesta V, Pliego-Alfaro F, Quesada MA, Mercado JA. Manipulation of strawberry fruit softening by antisense expression of a pectate lyase gene. Plant Physiol. 2002:**128**(2):751–759. https://doi.org/10.1104/pp.010671

Kim D, Langmead B, Salzberg SL. HISAT: a fast spliced aligner with low memory requirements. Nat Methods. 2015:**12**(4):357–360. https://doi.org/10.1038/nmeth.3317

Koeduka T, Fridman E, Gang DR, Vassao DG, Jackson BL, Kish CM, Orlova I, Spassova SM, Lewis NG, Noel JP, et al. Eugenol and isoeugenol, characteristic aromatic constituents of spices, are biosynthesized via reduction of a coniferyl alcohol ester. Proc Natl Acad Sci U S A. 2006:**103**(26):10128–10133. https://doi.org/10.1073/pnas.0603732103

Komis G, Samajova O, Ovecka M, Samaj J. Cell and developmental biology of plant mitogen-activated protein kinases. Annu Rev Plant Biol. 2018:**69**(1):237–265. https://doi.org/10.1146/annurev-arplant-042817-040314

Kondili M, Fust A, Preussner J, Kuenne C, Braun T, Looso M. UROPA: a tool for universal RObust peak annotation. Sci Rep. 2017:**7**(1):2593. https://doi.org/10.1038/s41598-017-02464-y

Kunieda T, Mitsuda N, Ohme-Takagi M, Takeda S, Aida M, Tasaka M, Kondo M, Nishimura M, Hara-Nishimura I. NAC family proteins NARS1/NAC2 and NARS2/NAM in the outer integument regulate embryogenesis in *Arabidopsis*. Plant Cell 2008:**20**(10):2631–2642. https://doi.org/10.1105/tpc.108.060160

Lei R, Qiao W, Hu F, Jiang H, Zhu S. A simple and effective method to encapsulate tobacco mesophyll protoplasts to maintain cell viability. MethodsX. 2015:**2**(11):24–32. https://doi.org/10.1016/j.mex.2014.11.004

Li BJ, Grierson D, Shi Y, Chen KS. Roles of abscisic acid in regulating ripening and quality of strawberry, a model non-climacteric fruit. Hortic Res. 2022:**9**(4):uhac089. https://doi.org/10.1093/hr/uhac089

Li C, Jia H, Chai Y, Shen Y. Abscisic acid perception and signaling transduction in strawberry: a model for non-climacteric fruit ripening. Plant Signal Behav. 2011:**6**(12):1950–1953. https://doi.org/10.4161/psb.6.12.18024

Li YH, Liu K, Tong GL, Xi C, Liu J, Zhao HP, Wang YD, Ren DT, Han SC. MPK3/MPK6-mediated Phosphorylation of ERF72 positively regulates resistance to *Botrytis cinerea* through directly and indirectly

activating the transcription of camalexin biosynthesis enzymes. J Exp Bot. 2022:**73**(1):413–428. https://doi.org/10.1093/jxb/erab415

Liang C, Wang Y, Zhu Y, Tang J, Hu B, Liu L, Ou S, Wu H, Sun X, Chu J, et al. OsNAP connects abscisic acid and leaf senescence by fine-tuning abscisic acid biosynthesis and directly targeting senescence-associated genes in rice. Proc Natl Acad Sci U S A. 2014:**111**(27):10013–10018. https://doi.org/10.1073/pnas.1321568111

Liao X, Li MS, Liu B, Yan ML, Yu XM, Zi HL, Liu RY, Yamamuro C. Interlinked regulatory loops of ABA catabolism and biosynthesis coordinate fruit growth and ripening in woodland strawberry. Proc Natl Acad Sci U S A. 2018:**115**(49):E11542–E11550. https://doi.org/10.1073/pnas.1812575115

Liao Y, Smyth GK, Shi W. Featurecounts: an efficient general purpose program for assigning sequence reads to genomic features. Bioinformatics 2014:**30**(7):923–930. https://doi.org/10.1093/bioinformatics/btt656

Lin-Wang K, Bolitho K, Grafton K, Kortstee A, Karunairetnam S, McGhie TK, Espley RV, Hellens RP, Allan AC. An R2R3 MYB transcription factor associated with regulation of the anthocyanin biosynthetic pathway in Rosaceae. BMC Plant Biol. 2010:**10**(1):50. https://doi.org/10.1186/1471-2229-10-50

Liu C, Yu H, Rao X, Li L, Dixon RA. Abscisic acid regulates secondary cell-wall formation and lignin deposition in *Arabidopsis thaliana* through phosphorylation of NST1. Proc Natl Acad Sci U S A. 2021:**118**(5):e2010911118. https://doi.org/10.1073/pnas.2010911118

Love MI, Huber W, Anders S. Moderated estimation of fold change and dispersion for RNA-seq data with DESeq2. Genome Biol. 2014:**15**(12):550. https://doi.org/10.1186/s13059-014-0550-8

Ma X, Zhang Q, Zhu Q, Liu W, Chen Y, Qiu R, Wang B, Yang Z, Li H, Lin Y, et al. A robust CRISPR/Cas9 system for convenient, high-efficiency multiplex genome editing in monocot and dicot plants. Mol Plant. 2015:**8**(8):1274–1284. https://doi.org/10.1016/j.molp.2015.04.007

Mao W, Han Y, Chen Y, Sun M, Feng Q, Li L, Liu L, Zhang K, Wei L, Han Z, et al. Low temperature inhibits anthocyanin accumulation in strawberry fruit by activating FvMAPK3-induced phosphorylation of FvMYB10 and degradation of Chalcone Synthase 1. Plant Cell 2022:**34**(4):1226–1249. https://doi.org/10.1093/plcell/koac006

Martin-Pizarro C, Vallarino JG, Osorio S, Meco V, Urrutia M, Pillet J, Casanal A, Merchante C, Amaya I, Willmitzer L, et al. The NAC transcription factor FaRIF controls fruit ripening in strawberry. Plant Cell 2021:**33**(5):1574–1593. https://doi.org/10.1093/plcell/koab070

Mattioli R, Francioso A, Mosca L, Silva P. Anthocyanins: a comprehensive review of their chemical properties and health effects on cardiovascular and neurodegenerative diseases. Molecules 2020:**25**(17):3809. https://doi.org/10.3390/molecules25173809

Medina-Puche L, Cumplido-Laso G, Amil-Ruiz F, Hoffmann T, Ring L, Rodriguez-Franco A, Caballero JL, Schwab W, Munoz-Blanco J, Blanco-Portales R. MYB10 Plays a major role in the regulation of flavonoid/phenylpropanoid metabolism during ripening of *Fragaria* × *ananassa* fruits. J Exp Bot. 2014:**65**(2):401–417. https://doi.org/10.1093/jxb/ert377

Molina-Hidalgo FJ, Medina-Puche L, Canete-Gomez C, Franco-Zorrilla JM, Lopez-Vidriero I, Solano R, Caballero JL, Rodriguez-Franco A, Blanco-Portales R, Munoz-Blanco J, et al. The fruit-specific transcription factor FaDOF2 regulates the production of eugenol in ripe fruit receptacles. J Exp Bot. 2017:**68**(16):4529–4543. https://doi.org/10.1093/jxb/erx257

Moya-Leon MA, Mattus-Araya E, Herrera R. Molecular events occurring during softening of strawberry fruit. Front Plant Sci. 2019:**10**(5):615. https://doi.org/10.3389/fpls.2019.00615

Nakagami H, Pitzschke A, Hirt H. Emerging MAP kinase pathways in plant stress signalling. Trends Plant Sci. 2005:**10**(7):339–346. https://doi.org/10.1016/j.tplants.2005.05.009

Nakayama T, Takahashi S, Waki T. Formation of flavonoid metabolons: functional significance of protein-protein interactions and impact on flavonoid chemodiversity. Front Plant Sci. 2019:**10**(7):821. https://doi.org/10.3389/fpls.2019.00821

Nishida H, Nosaki S, Suzuki T, Ito M, Miyakawa T, Nomoto M, Tada Y, Miura K, Tanokura M, Kawaguchi M, et al. Different DNA-binding specificities of NLP and NIN transcription factors underlie nitrate-induced control of root nodulation. Plant Cell 2021:**33**(7):2340–2359. https://doi.org/10.1093/plcell/koab103

O'Malley RC, Huang SC, Song L, Lewsey MG, Bartlett A, Nery JR, Galli M, Gallavotti A, Ecker JR. Cistrome and epicistrome features shape the regulatory DNA landscape. Cell 2016:**165**(5):1280–1292. https://doi.org/10.1016/j.cell.2016.04.038

Olsen AN, Ernst HA, Lo Leggio L, Skriver K. NAC Transcription factors: structurally distinct, functionally diverse. Trends Plant Sci. 2005:**10**(2):79–87. https://doi.org/10.1016/j.tplants.2004.12.010

Oosumi T, Gruszewski HA, Blischak LA, Baxter AJ, Wadl PA, Shuman JL, Veilleux RE, Shulaev V. High-efficiency transformation of the diploid strawberry (*Fragaria vesca*) for functional genomics. Planta 2006:**223**(6):1219–1230. https://doi.org/10.1007/s00425-005-0170-3

Paniagua C, Blanco-Portales R, Barcelo-Munoz M, Garcia-Gago JA, Waldron KW, Quesada MA, Munoz-Blanco J, Mercado JA. Antisense down-regulation of the strawberry beta-galactosidase gene FabetaGal4 increases cell wall galactose levels and reduces fruit softening. J Exp Bot. 2016:**67**(3):619–631. https://doi.org/10.1093/jxb/erv462

Paniagua C, Pose S, Morris VJ, Kirby AR, Quesada MA, Mercado JA. Fruit softening and pectin disassembly: an overview of nanostructural pectin modifications assessed by atomic force microscopy. Ann Bot. 2014:**114**(6):1375–1383. https://doi.org/10.1093/aob/mcu149

Pi M, Hu S, Cheng L, Zhong R, Cai Z, Liu Z, Yao JL, Kang C. The MADS-box gene FveSEP3 plays essential roles in flower organogenesis and fruit development in woodland strawberry. Hortic Res. 2021:**8**(1):247. https://doi.org/10.1038/s41438-021-00673-1

Quesada MA, Blanco-Portales R, Pose S, Garcia-Gago JA, Jimenez-Bermudez S, Munoz-Serrano A, Caballero JL, Pliego-Alfaro F, Mercado JA, Munoz-Blanco J. Antisense down-regulation of the FaPG1 gene reveals an unexpected central role for polygalacturonase in strawberry fruit softening. Plant Physiol. 2009:**150**(2):1022–1032. https://doi.org/10.1104/pp.109.138297

Riechmann JL, Heard J, Martin G, Reuber L, Jiang CZ, Keddie J, Adam L, Pineda O, Ratcliffe OJ, Samaha RR, et al. *Arabidopsis* transcription factors: genome-wide comparative analysis among eukaryotes. Science 2000:**290**(5499):2105–2110. https://doi.org/10.1126/science.290.5499.2105

Robinson JT, Thorvaldsdottir H, Winckler W, Guttman M, Lander ES, Getz G, Mesirov JP. Integrative genomics viewer. Nat Biotechnol. 2011:**29**(1):24–26. https://doi.org/10.1038/nbt.1754

Sanchez-Gomez C, Pose D, Martin-Pizarro C. Insights into transcription factors controlling strawberry fruit development and ripening. Front Plant Sci. 2022:**13**(10):1022369. https://doi.org/10.3389/fpls.2022.1022369

Saravanan RS, Rose JK. A critical evaluation of sample extraction techniques for enhanced proteomic analysis of recalcitrant plant tissues. Proteomics 2004:**4**(9):2522–2532. https://doi.org/10.1002/pmic.200300789

Schaart JG, Dubos C, Romero De La Fuente I, van Houwelingen AM, de Vos RC, Jonker HH, Xu W, Routaboul JM, Lepiniec L, Bovy AG. Identification and characterization of MYB-bHLH-WD40 regulatory complexes controlling proanthocyanidin biosynthesis in strawberry (*Fragaria* × *ananassa*) fruits. New Phytol. 2013:**197**(2):454–467. https://doi.org/10.1111/nph.12017

Seymour GB, Ryder CD, Cevik V, Hammond JP, Popovich A, King GJ, Vrebalov J, Giovannoni JJ, Manning K. A SEPALLATA gene is involved in the development and ripening of strawberry (*Fragaria* × *ananassa* Duch.) fruit, a non-climacteric tissue. J Exp Bot. 2011:**62**(3):1179–1188. https://doi.org/10.1093/jxb/erq360

Shahnejat-Bushehri S, Tarkowska D, Sakuraba Y, Balazadeh S. *Arabidopsis* NAC transcription factor JUB1 regulates GA/BR metabolism and signalling. Nat Plants. 2016:**2**(3):16013. https://doi.org/10.1038/nplants.2016.13

Shan W, Kuang JF, Chen L, Xie H, Peng HH, Xiao YY, Li XP, Chen WX, He QG, Chen JY, et al. Molecular characterization of banana NAC transcription factors and their interactions with ethylene signalling component EIL during fruit ripening. J Exp Bot. 2012:**63**(14): 5171–5187. https://doi.org/10.1093/jxb/ers178

Simpson SD, Nakashima K, Narusaka Y, Seki M, Shinozaki K, Yamaguchi-Shinozaki K. Two different novel cis-acting elements of erd1, a clpA homologous *Arabidopsis* gene function in induction by dehydration stress and dark-induced senescence. Plant J. 2003:**33**(2): 259–270. https://doi.org/10.1046/j.1365-313X.2003.01624.x

Soma F, Takahashi F, Suzuki T, Shinozaki K, Yamaguchi-Shinozaki K. Plant Raf-like kinases regulate the mRNA population upstream of ABA-unresponsive SnRK2 kinases under drought stress. Nat Commun. 2020:**11**(1):1373. https://doi.org/10.1038/s41467-020-15239-3

Sparkes IA, Runions J, Kearns A, Hawes C. Rapid, transient expression of fluorescent fusion proteins in tobacco plants and generation of stably transformed plants. Nat Protoc. 2006:**1**(4):2019–2025. https://doi.org/10.1038/nprot.2006.286

Stanko V, Giuliani C, Retzer K, Djamei A, Wahl V, Wurzinger B, Wilson C, Heberle-Bors E, Teige M, Kragler F. Timing is everything: highly specific and transient expression of a MAP kinase determines auxin-induced leaf venation patterns in *Arabidopsis*. Mol Plant. 2014:**7**(11):1637–1652. https://doi.org/10.1093/mp/ssu080

Thompson JD, Gibson TJ, Plewniak F, Jeanmougin F, Higgins DG. The CLUSTAL_X windows interface: flexible strategies for multiple sequence alignment aided by quality analysis tools. Nucleic Acids Res. 1997:**25**(24):4876–4882. https://doi.org/10.1093/nar/25.24.4876

Tisza V, Kovács L, Balogh A, Heszky L, Kiss E. Characterization of *FaSPT*, a *SPATULA* gene encoding a bHLH transcriptional factor from the non-climacteric strawberry fruit. Plant Physiol Biochem. 2010:**48**(10–11):822–826. https://doi.org/10.1016/j.plaphy.2010.08.001

Vallarino JG, Merchante C, Sanchez-Sevilla JF, de Luis Balaguer MA, Pott DM, Ariza MT, Casanal A, Pose D, Vioque A, Amaya I, et al. Characterizing the involvement of FaMADS9 in the regulation of strawberry fruit receptacle development. Plant Biotechnol J. 2020:**18**(4):929–943. https://doi.org/10.1111/pbi.13257

Vrebalov J, Ruezinsky D, Padmanabhan V, White R, Medrano D, Drake R, Schuch W, Giovannoni J. A MADS-box gene necessary for fruit ripening at the tomato ripening-inhibitor (rin) locus. Science 2002:**296**(5566):343–346. https://doi.org/10.1126/science.1068181

Wang DD, Yeats TH, Uluisik S, Rose JKC, Seymour GB. Fruit softening: revisiting the role of pectin. Trends Plant Sci. 2018:**23**(4):302–310. https://doi.org/10.1016/j.tplants.2018.01.006

Wang J, Tian S, Yu Y, Ren Y, Guo S, Zhang J, Li M, Zhang H, Gong G, Wang M, et al. Natural variation in the NAC transcription factor NONRIPENING contributes to melon fruit ripening. J Integr Plant Biol. 2022:**64**(7):1448–1461. https://doi.org/10.1111/jipb.13278

Wang J, Wang Y, Zhang J, Ren Y, Li M, Tian S, Yu Y, Zuo Y, Gong G, Zhang H, et al. The NAC transcription factor ClNAC68 positively regulates sugar content and seed development in watermelon by repressing ClINV and ClGH3.6. Hortic Res. 2021:**8**(1):214. https://doi.org/10.1038/s41438-021-00649-1

Wang P, Wang Y, Wang W, Chen T, Tian S, Qin G. Ubiquitination of phytoene synthase 1 precursor modulates carotenoid biosynthesis in tomato. Commun Biol. 2020:**3**(1):730. https://doi.org/10.1038/s42003-020-01474-3

Wang S, Wang T, Li Q, Xu C, Tian J, Wang Y, Zhang X, Xu X, Han Z, Wu T. Phosphorylation of MdERF17 by MdMPK4 promotes apple fruit peel degreening during light/dark transitions. Plant Cell 2022:**34**(5):1980–2000. https://doi.org/10.1093/plcell/koac049

Wang Y, Wang W, Cai J, Zhang Y, Qin G, Tian S. Tomato nuclear proteome reveals the involvement of specific E2 ubiquitin-conjugating enzymes in fruit ripening. Genome Biol. 2014:**15**(12): 548. https://doi.org/10.1186/s13059-014-0548-2

Wei L, Mao W, Jia M, Xing S, Ali U, Zhao Y, Chen Y, Cao M, Dai Z, Zhang K, et al. FaMYB44.2, a transcriptional repressor, negatively regulates sucrose accumulation in strawberry receptacles through interplay with FaMYB10. J Exp Bot. 2018:**69**(20):4805–4820. https://doi.org/10.1093/jxb/ery249

Wu CJ, Shan W, Liu XC, Zhu LS, Wei W, Yang YY, Guo YF, Bouzayen M, Chen JY, Lu WJ, et al. Phosphorylation of transcription factor bZIP21 by MAP kinase MPK6-3 enhances banana fruit ripening. Plant Physiol. 2022:**188**(3):1665–1685. https://doi.org/10.1093/plphys/kiab539

Wu VW, Thieme N, Huberman LB, Dietschmann A, Kowbel DJ, Lee J, Calhoun S, Singan VR, Lipzen A, Xiong Y, et al. The regulatory and transcriptional landscape associated with carbon utilization in a filamentous fungus. Proc Natl Acad Sci U S A. 2020:**117**(11):6003–6013. https://doi.org/10.1073/pnas.1915611117

Xiang Y, Bian X, Wei T, Yan J, Sun X, Han T, Dong B, Zhang G, Li J, Zhang A. ZmMPK5 phosphorylates ZmNAC49 to enhance oxidative stress tolerance in maize. New Phytol. 2021:**232**(6):2400–2417. https://doi.org/10.1111/nph.17761

Yi S, Mao JX, Zhang XY, Li XM, Zhang ZH, Li H. *FveARF2* negatively regulates fruit ripening and quality in strawberry. Front Plant Sci. 2022:**13**(10):1023739. https://doi.org/10.3389/fpls.2022.1023739

Yip Delormel T, Boudsocq M. Properties and functions of calcium-dependent protein kinases and their relatives in *Arabidopsis thaliana*. New Phytol. 2019:**224**(2):585–604. https://doi.org/10.1111/nph.16088

Zhang Y, Butelli E, Martin C. Engineering anthocyanin biosynthesis in plants. Curr Opin Plant Biol. 2014:**19**(6):81–90. https://doi.org/10.1016/j.pbi.2014.05.011

Zhang Z, Dong J, Ji C, Wu Y, Messing J. NAC-type transcription factors regulate accumulation of starch and protein in maize seeds. Proc Natl Acad Sci U S A. 2019:**116**(23):11223–11228. https://doi.org/10.1073/pnas.1904995116

Zhang Y, Liu T, Meyer CA, Eeckhoute J, Johnson DS, Bernstein BE, Nusbaum C, Myers RM, Brown M, Li W, et al. Model-based analysis of ChIP-Seq (MACS). Genome Biol. 2008:**9**(9):R137. https://doi.org/10.1186/gb-2008-9-9-r137

Zhang M, Su J, Zhang Y, Xu J, Zhang S. Conveying endogenous and exogenous signals: MAPK cascades in plant growth and defense. Curr Opin Plant Biol. 2018:**45**(Pt A):1–10. https://doi.org/10.1016/j.pbi.2018.04.012

Zhou H, Lin-Wang K, Wang H, Gu C, Dare AP, Espley RV, He H, Allan AC, Han Y. Molecular genetics of blood-fleshed peach reveals activation of anthocyanin biosynthesis by NAC transcription factors. Plant J. 2015:**82**(1):105–121. https://doi.org/10.1111/tpj.12792

Zhou H, Ren S, Han Y, Zhang Q, Qin L, Xing Y. Identification and analysis of mitogen-activated protein kinase (MAPK) cascades in *Fragaria vesca*. Int J Mol Sci. 2017:**18**(8):1766. https://doi.org/10.3390/ijms18081766

Zhou L, Tang R, Li X, Tian S, Li B, Qin G. N^6-methyladenosine RNA modification regulates strawberry fruit ripening in an ABA-dependent manner. Genome Biol. 2021:**22**(1):168. https://doi.org/10.1186/s13059-021-02385-0